

國立交通大學

電信工程學系

碩士論文

無線感測器網路下之結合通道估計與感測
器容錯碼的設計

Combined Channel Estimation and Sensor Fault
Protection in Wireless Sensor Networks

研究生：黃錫堯

指導教授：陳伯寧 教授

中華民國九十七年七月

中文摘要

無線感測器網路常設置在惡劣的環境中，因此感測器有可能會出現無預警的故障而導致接收端(fusion center)對環境判斷的準確度不穩定。針對此種情況，最直接的方式就是感測器先傳送訓練碼(training sequences)讓接收端去偵測是否有感測器發生故障，但此動作會增加感測器所消耗的能量，而導致由電池來供應電源的感測器運作壽命降低。

在此論文中，我們運用編碼的技巧來使無線感測器網路能同時擁有通道估計與感測器容錯的能力，我們將運用模擬退火法(simulation annealing)來尋找達到最小的錯誤率聯集上限(union bound)的最佳非線性碼。之後，我們採用量化器來對抗通道嚴重衰減(deep fading)的情況。模擬結果顯示，我們的方法可以在不考慮感測器故障、通道估計和等化的情況下，即可於效能上媲美於有傳送訓練碼的系統。



Abstract

Wireless sensor networks are usually deployed in a harsh environment. Hence, the performance of the final decision at the fusion center is not stable because some of the sensors may be unexpectedly faulty. A straightforward technique to exclude untrustworth observations from faulty sensors at the fusion center is to detect them based on the pre-sent training sequences. However, the transmission of training sequences consumes additional energy, and shortens the life cycle of the battery-supported sensors.

In this thesis, we proposed to combine channel estimation and sensor fault protection in wireless sensor networks in terms of the coding technique. Simulation annealing is employed to search the best non-linear code that minimizes the upper error bound. Quantization is later added in order to eliminate the sudden performance degradation due to deep fading. Our results show that the proposed combined scheme can compete with the the conventional training-sequence-based fusion in performance but without the effort of faulty-sensor detection, channel estimation and equalization.

Acknowledgements

I am deeply grateful to everyone who help me to finish the thesis.

To my advisor, Professor Chen, for your patient instruction and brilliance guidance throughout the research. This work would not been possible without your advise and commitment. I learn a lot from you. It is my pleasure to be advised by you.

To Professors Han and Wang, thanks for your opinions and explanation in our meeting. You make me understand more about the research topic.

To my lab mates, you always listen to my problem, give me much help and more advises, and encourage me when I am depressed.

And thanks National Chiao-Tung University for providing such good environment and such many resource for me.

In the end, I would like to dedicate this thesis to my family, for their support, love and encourage all the time.

Contents

List of Tables	iv
List of Figures	v
1 Introduction	1
2 Preliminaries	3
2.1 System Models	3
2.2 Pairwise-Error-Probability Union Bound Under Rayleigh Fadings	5
2.2.1 Union Bound Under Rayleigh Fadings With Perfect Sensor Observations	10
2.2.2 Union Bound Under Rayleigh Fadings With Faulty Sensors	10
2.3 Code Search	11
3 Simulation Results	15
3.1 Parameter Determination for Least Square (LS) Estimation	15
3.2 Deep Fade Effect Due to Soft-Decision	17
4 Amendment to Deep Fading by Quantization	68

4.1	Quantization of The Reception	69
4.2	Quantization of the Reception Product	75
5	Conclusions	81
	Bibliography	82



List of Tables

3.1 The SNRs corresponding to sudden performance degradation of the COM scheme. 19

4.1 The optimum uniform step size for gaussian random variable 69



List of Figures

2.1	System model of wireless sensor networks	4
2.2	The bounds in (2.11) (red points) and (2.12) (green points) for sixty different codes.	13
2.3	Performances of the best codes searched in terms of different union bound criterions.	14
3.1	Performances of hypothesis detection based on LS estimate of channel coefficients in terms of training sequences. Ten sensors, each transmitting ten bits, and two hypotheses are assumed. In the legend, $LS(x, y)$ represents that x training bits and y code bits are transmitted.	16
3.2	Performances of hypothesis detection. “S3H2” represents three sensors and two hypotheses are assumed in this figure.	20
3.3	Performances of hypothesis detection. “S5H2” represents five sensors and two hypotheses are assumed in this figure.	21
3.4	Performances of hypothesis detection. “S8H2” represents eight sensors and two hypotheses are assumed in this figure.	22
3.5	Performances of hypothesis detection. “S10H2” represents ten sensors and two hypotheses are assumed in this figure.	23

3.6	Performances of hypothesis detection. “N10H2” represents 10 bits per sensor and two hypotheses are assumed in this figure.	24
3.7	Performances of hypothesis detection. “N15H2” represents 15 bits per sensor and two hypotheses are assumed in this figure.	25
3.8	Performances of hypothesis detection. “N20H2” represents 20 bits per sensor and two hypotheses are assumed in this figure.	26
3.9	Performances of hypothesis detection. “N25H2” represents 25 bits per sensor and two hypotheses are assumed in this figure.	27
3.10	Performances of hypothesis detection. “S3H2 hard decision” represents three sensors, two hypotheses, hard-decision fusion are assumed in this figure. . .	28
3.11	Performances of hypothesis detection. “S5H2 hard decision” represents five sensors, two hypotheses, hard-decision fusion are assumed in this figure. . .	29
3.12	Performances of hypothesis detection. “S8H2 hard decision” represents eight sensors, two hypotheses, hard-decision fusion are assumed in this figure. . .	30
3.13	Performances of hypothesis detection. “S10H2 hard decision” represents ten sensors, two hypotheses, hard-decision fusion are assumed in this figure. . .	31
3.14	Performance of hypothesis detection. “S3H2 random fault” represents three sensors, two hypotheses and one random faulty sensor are assumed in this figure.	32
3.15	Performance of hypothesis detection. “S5H2 random fault” represents five sensors, two hypotheses and one random faulty sensor are assumed in this figure.	33

3.16 Performance of hypothesis detection. “S8H2 random fault” represents eight sensors, two hypotheses and one random faulty sensor are assumed in this figure.	34
3.17 Performance of hypothesis detection. “S10H2 random fault” represents ten sensors, two hypotheses and one random faulty sensor are assumed in this figure.	35
3.18 Performance of hypothesis detection. “N10H2 random fault” represents 10 bits per sensor, two hypotheses and one random faulty sensor are assumed in this figure.	36
3.19 Performance of hypothesis detection. “N15H2 random fault” represents 15 bits per sensor, two hypotheses and one random faulty sensor are assumed in this figure.	37
3.20 Performance of hypothesis detection. “N20H2 random fault” represents 20 bits per sensor, two hypotheses and one random faulty sensor are assumed in this figure.	38
3.21 Performance of hypothesis detection. “N25H2 random fault” represents 25 bits per sensor, two hypotheses and one random faulty sensor are assumed in this figure.	39
3.22 Performance of hypothesis detection. “S3H2 random fault(without sensor fault detection)” represents three sensors, two hypotheses, one random faulty sensor, and no faulty-sensor detection at the LSE fusion are assumed in this figure.	40



3.23 Performance of hypothesis detection. “S5H2 random fault(without sensor fault detection)” represents five sensors, two hypotheses, one random faulty sensor, and no faulty-sensor detection at the LSE fusion are assumed in this figure.	41
3.24 Performance of hypothesis detection. “S8H2 random fault(without sensor fault detection)” represents eight sensors, two hypotheses, one random faulty sensor, and no faulty-sensor detection at the LSE fusion are assumed in this figure.	42
3.25 Performance of hypothesis detection. “S10H2 random fault(without sensor fault detection)” represents ten sensors, two hypotheses, one random faulty sensor, and no faulty-sensor detection at the LSE fusion are assumed in this figure.	43
3.26 Performance of hypothesis detection. “S10N10H2” represents ten sensors, 10 bits per sensor and two hypotheses are assumed in this figure.	44
3.27 Performance of hypothesis detection. “S10N15H2” represents ten sensors, 15 bits per sensor and two hypotheses are assumed in this figure.	45
3.28 Performance of hypothesis detection. “S10N20H2” represents ten sensors, 20 bits per sensor and two hypotheses are assumed in this figure.	46
3.29 Performance of hypothesis detection. “S10N25H2” represents ten sensors, 25 bits per sensor and two hypotheses are assumed in this figure.	47
3.30 Performances of hypothesis detection. “S3H4” represents three sensors and four hypotheses are assumed in this figure.	48
3.31 Performances of hypothesis detection. “S5H4” represents five sensors and four hypotheses are assumed in this figure.	49

3.32	Performances of hypothesis detection. “S8H4” represents eight sensors and four hypotheses are assumed in this figure.	50
3.33	Performances of hypothesis detection. “S10H4” represents ten sensors and four hypotheses are assumed in this figure.	51
3.34	Performances of hypothesis detection. “N10H4” represents 10 bits per sensor and four hypotheses are assumed in this figure.	52
3.35	Performances of hypothesis detection. “N15H4” represents 15 bits per sensor and four hypotheses are assumed in this figure.	53
3.36	Performances of hypothesis detection. “N20H4” represents 20 bits per sensor and four hypotheses are assumed in this figure.	54
3.37	Performances of hypothesis detection. “N25H4” represents 25 bits per sensor and four hypotheses are assumed in this figure.	55
3.38	Performance of hypothesis detection. “S3H4 random fault” represents three sensors, four hypotheses and one random faulty sensor are assumed in this figure.	56
3.39	Performance of hypothesis detection. “S5H4 random fault” represents five sensors, four hypotheses and one random faulty sensor are assumed in this figure.	57
3.40	Performance of hypothesis detection. “S8H4 random fault” represents eight sensors, four hypotheses and one random faulty sensor are assumed in this figure.	58
3.41	Performance of hypothesis detection. “S10H4 random fault” represents ten sensors, four hypotheses and one random faulty sensor are assumed in this figure.	59

3.42	Performance of hypothesis detection. “N10H4 random fault” represents 10 bits per sensor, four hypotheses and one random faulty sensor are assumed in this figure.	60
3.43	Performance of hypothesis detection. “N15H4 random fault” represents 15 bits per sensor, four hypotheses and one random faulty sensor are assumed in this figure.	61
3.44	Performance of hypothesis detection. “N20H4 random fault” represents 20 bits per sensor, four hypotheses and one random faulty sensor are assumed in this figure.	62
3.45	Performance of hypothesis detection. “N25H4 random fault” represents 25 bits per sensor, four hypotheses and one random faulty sensor are assumed in this figure.	63
3.46	Performance of hypothesis detection. “S10N10H4” represents ten sensors, 10 bits per sensor and four hypotheses are assumed in this figure.	64
3.47	Performance of hypothesis detection. “S10N15H4” represents ten sensors, 15 bits per sensor and four hypotheses are assumed in this figure.	65
3.48	Performance of hypothesis detection. “S10N20H4” represents ten sensors, 20 bits per sensor and four hypotheses are assumed in this figure.	66
3.49	Performance of hypothesis detection. “S10N25H4” represents ten sensors, 25 bits per sensor and four hypotheses are assumed in this figure.	67
4.1	Performance of quantized and soft-decision COM fusions. “S10H2” represents ten sensors and two hypotheses are assumed in this figure. “3bitsQ(\mathbf{r})” means 3-bit quantizer is used in the quantization of reception \mathbf{r}	70

4.2	Performance of 3-bit quantized COM fusion and LSE fusion. “S10H2” represents ten sensors and two hypotheses are assumed in this figure. “3bitsQ(\mathbf{r})” means 3-bit quantizer is used in the quantization of reception \mathbf{r}	71
4.3	Performance of 3-bit quantized COM fusion and LSE fusion. “S10H2 . . . (random fault)” represents ten sensors, two hypotheses and one random faulty sensor are assumed in this figure. “3bitsQ(\mathbf{r})” means 3-bit quantizer is used in the quantization of reception \mathbf{r}	72
4.4	Performance of 3-bit quantized COM fusion and 3-bit quantized LSE fusion. “S10H2” represents ten sensors and two hypotheses are assumed in this figure. “3bitsQ(\mathbf{r})” means 3-bit quantizer is used in the quantization of reception \mathbf{r}	73
4.5	Performance of 3-bit quantized COM fusion and 3-bit quantized LSE fusion. “S10H2 . . . (random fault)” represents ten sensors, two hypotheses and one random faulty sensor are assumed in this figure. “3bitsQ(\mathbf{r})” means 3-bit quantizer is used in the quantization of reception \mathbf{r}	74
4.6	Performance of reception-quantized and reception-product quantized COM fusions. “S10H2” represents ten sensors and two hypotheses are assumed in this figure. “3bitsQ(\mathbf{r})” 3-bit quantizer is used in the quantization of reception \mathbf{r} , while “3bitsQ($\mathbf{r}\mathbf{r}^H$)” means 3-bit quantizer is used in the quantization of product reception $\mathbf{r}\mathbf{r}^H$	76
4.7	Performance of 3-bit reception-product-quantized COM fusion and LSE fusion. “S10H2” represents ten sensors and two hypotheses are assumed in this figure. “3bitsQ($\mathbf{r}\mathbf{r}^H$)” means 3-bit quantizer is used in the quantization of product reception $\mathbf{r}\mathbf{r}^H$	77

4.8 Performance of 3-bit product-quantized COM fusion and LSE fusion. “S10H2
 . . . (random fault)” represents ten sensors, two hypotheses and one random
 faulty sensor are assumed in this figure. “3bitsQ(rr^H)” means 3-bit quantizer
 is used in the quantization of product reception rr^H 78

4.9 Performance of 3-bit reception-product-quantized COM fusion and 3-bit quan-
 tized LSE fusion. “S10H2” represents ten sensors and two hypotheses are
 assumed in this figure. “3bitsQ(rr^H)” means 3-bit quantizer is used in the
 quantization of product reception rr^H 79

4.10 Performance of 3-bit reception-product-quantized COM fusion and 3-bit quan-
 tized LSE fusion. “S10H2 . . . (random fault)” represents ten sensors, two hy-
 potheses and one random faulty sensor are assumed in this figure. “3bitsQ(rr^H)”
 means 3-bit quantizer is used in the quantization of product reception rr^H . . . 80



Chapter 1

Introduction

The wireless sensor network consists of a number of sensors to, e.g. detect the environmental variations, and then transmit or relay the detection results to the base station. The base station, serving as a fusion center, determines what phenomenon has occurred after the collection of these information. A wireless sensor network must be able to function under severe conditions so as to work in a fireplace, jungle, polluted area, or some harsh environment. As a result, the channel of the wireless sensor network should be a noisy one. Moreover, the sensors may be nearly out-of-battery or even faulty, and incorrect information may be received by the base station [1, 2, 4, 5, 9]. This motivates our research to search for an error correcting code for use of the wireless sensor network with acceptable performance that is robust to sensor faults [3, 12].

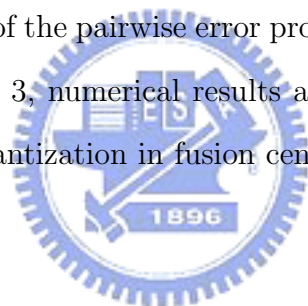
A straightforward method to prevent the performance degradation from unexpected sensor faults in a time-varying environment is to transmit a sequence of training bits for faulty sensor detection. However, the drawback of this method is that part of the transmission energy that is precious to the battery-supported sensors will be consumed by transmitting the training sequence.

In 2002, Skoglund et al proposed to use computer-searched nonlinear codes for combined

channel estimation and error protection in the slow fading channels [10] in order to release the power consumption on the training sequence. The nonlinear codes were searched by way of the simulated annealing technique [8]. They found under the presumption of fixed effective code rate that the best non-linear code will result in apparently better performance than a benchmark system with a certain number of training bits. In certain cases, performance improvement can be up to 2 dB.

In this thesis, we consider to apply Skoglund's concept to the wireless sensor networks, i.e. to search for the best code design for combined channel estimation and sensor-fault protection. The objective is to provide good fault-tolerant capability for the wireless sensor networks.

The rest of the thesis is organized as follows. In Chapter 2, we will introduce the system model, derive the union bound of the pairwise error probability, and characterize the method of the code search. In Chapter 3, numerical results are presented, followed by remarks on these results. In Chapter 4, quantization in fusion center. Summary and conclusion appear in Chapter 5.

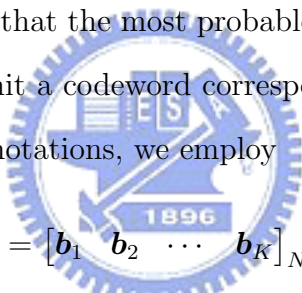


Chapter 2

Preliminaries

2.1 System Models

In the system we considered, there are M environmental hypotheses, H_1, H_2, \dots, H_M , and K sensors. When a sensor realizes that the most probable hypothesis is H_ℓ upon the reception of its observation, it will transmit a codeword corresponding to hypothesis H_ℓ according to the pre-designed codebook. In notations, we employ


$$\mathbb{C} = [\mathbf{b}_1 \ \mathbf{b}_2 \ \cdots \ \mathbf{b}_K]_{N \times K}$$

to represent the transmitted code matrix of the K wireless sensors, where

$$\mathbf{b}_i = \begin{bmatrix} b_{i,1} \\ b_{i,2} \\ \vdots \\ b_{i,N} \end{bmatrix}$$

is the transmitted codeword of sensor i , and $\mathbf{b}_i \in \{\pm 1\}^N$. Given that the true hypothesis is H_ℓ , the probability of sensor i favoring hypothesis $H_{\bar{\ell}}$ is denoted by $P_{\bar{\ell}| \ell}^{(i)}$.

The received complex matrix at the fusion center is

$$\mathbb{R} = [\mathbf{r}_1 \ \mathbf{r}_2 \ \cdots \ \mathbf{r}_K]_{L \times K},$$

Multiclass phenomenon

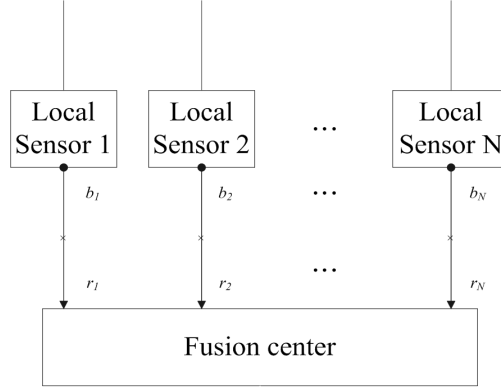


Figure 2.1: System model of wireless sensor networks

where

$$\mathbf{r}_i = \begin{bmatrix} h_{i,1} & 0 & 0 & 0 & \cdots & 0 \\ \vdots & \ddots & \ddots & \ddots & \ddots & \vdots \\ h_{i,P} & \cdots & h_{i,1} & 0 & \cdots & 0 \\ 0 & h_{i,P} & \cdots & h_{i,1} & \cdots & \vdots \\ \vdots & \vdots & \ddots & \ddots & \ddots & 0 \\ 0 & \cdots & 0 & h_{i,P} & \cdots & h_{i,1} \\ \vdots & \ddots & \ddots & \ddots & \ddots & \vdots \\ 0 & 0 & 0 & \cdots & 0 & h_{i,P} \end{bmatrix}_{L \times N} \mathbf{b}_i + \mathbf{n}_i, \quad (2.1)$$

$L = N + P - 1$, the channel coefficients

$$\mathbf{h}_i = \begin{bmatrix} h_{i,1} \\ \vdots \\ h_{i,P} \end{bmatrix}$$

are assumed constant over the transmission of codeword \mathbf{b}_i , and \mathbf{n}_i is the zero-mean complex Gaussian noise over the i th wireless channel link. It can be easily verified that we can change Eq. (2.1) to:

$$\mathbf{r}_i = \mathbb{B}_i \mathbf{h}_i + \mathbf{n}_i,$$

where

$$\mathbb{B}_i = \begin{bmatrix} b_{i,1} & 0 & \cdots & 0 \\ b_{i,2} & b_{i,1} & \cdots & 0 \\ \vdots & \ddots & \ddots & \vdots \\ b_{i,P} & b_{i,P-1} & \cdots & b_{i,1} \\ \vdots & \ddots & \ddots & \vdots \\ b_{i,N} & b_{i,N-1} & & b_{N-P+1} \\ \vdots & \ddots & \ddots & \vdots \\ 0 & 0 & \cdots & b_{i,N} \end{bmatrix}_{L \times P}$$

As a result,

$$\mathbb{R} = [\mathbf{r}_1 \quad \mathbf{r}_2 \quad \cdots \quad \mathbf{r}_K] = [\mathbb{B}_1 \mathbf{h}_1 \quad \mathbb{B}_2 \mathbf{h}_2 \quad \cdots \quad \mathbb{B}_K \mathbf{h}_K] + \mathbb{N}$$

where $\mathbb{N} = [\mathbf{n}_1 \quad \mathbf{n}_2 \quad \cdots \quad \mathbf{n}_K]$.

Based upon the received matrix \mathbb{R} , the maximum-likelihood (ML) decision for the true hypothesis is given by:

$$\begin{aligned} \hat{\ell} &= \arg \min_{1 \leq \ell \leq M} \sum_{k=1}^K \left\| \mathbf{r}_k - \mathbb{B}_k^{(\ell)} \mathbf{h}_k \right\|^2 \\ &= \arg \min_{1 \leq \ell \leq M} \sum_{k=1}^K \left\| \mathbf{r}_k - \mathbb{P}_{B_k}^{(\ell)} \mathbf{r}_k \right\|^2, \end{aligned} \quad (2.2)$$

where $\mathbb{P}_{B_k}^{(\ell)} = \mathbb{B}_k^{(\ell)} [(\mathbb{B}_k^{(\ell)})^T \mathbb{B}_k^{(\ell)}]^{-1} (\mathbb{B}_k^{(\ell)})^T$, and the non-zero column components of matrix $\mathbb{B}_k^{(\ell)}$ is the codeword $\mathbf{b}_k^{(\ell)}$ for sensor k with respect to hypothesis H_ℓ .

2.2 Pairwise-Error-Probability Union Bound Under Rayleigh Fadings

In this section, we derive the pairwise error probability bound of the wireless sensor network considered.

The detection error P_e at the fusion center can be given by:

$$P_e = \sum_{m=1}^M \Pr(H_m) \Pr(\hat{\ell} \neq m | H_m).$$

Then, by denoting the local decision at sensor i by s_i , we obtain:

$$\begin{aligned}
& \Pr(\hat{\ell} \neq m | H_m) \\
&= \sum_{\ell_1=1}^M \sum_{\ell_2=1}^M \cdots \sum_{\ell_K=1}^M \Pr(\hat{\ell} \neq m | H_m, s_1 = H_{\ell_1}, s_2 = H_{\ell_2}, \cdots, s_K = H_{\ell_K}) \\
&\quad \times \Pr(s_1 = H_{\ell_1}, s_2 = H_{\ell_2}, \cdots, s_K = H_{\ell_K} | H_m) \\
&= \sum_{\ell_1=1}^M \sum_{\ell_2=1}^M \cdots \sum_{\ell_K=1}^M \Pr(\hat{\ell} \neq m | H_m, s_1 = H_{\ell_1}, s_2 = H_{\ell_2}, \cdots, s_K = H_{\ell_K}) \\
&\quad \times \Pr(s_1 = H_{\ell_1} | H_m) \Pr(s_2 = H_{\ell_2} | H_m) \cdots \Pr(s_K = H_{\ell_K} | H_m) \\
&= \sum_{\ell_1=1}^M \sum_{\ell_2=1}^M \cdots \sum_{\ell_K=1}^M \Pr(\hat{\ell} \neq m | H_m, s_1 = H_{\ell_1}, s_2 = H_{\ell_2}, \cdots, s_K = H_{\ell_K}) P_{\ell_1|m}^{(1)} P_{\ell_2|m}^{(2)} \cdots P_{\ell_K|m}^{(K)}
\end{aligned} \tag{2.3}$$

Because the true hypothesis H_m , the transmitted code matrix at the local sensors, and the received code matrix at the fusion center form a Markov chain, $\Pr(\hat{\ell} \neq m | H_m, s_1 = H_{\ell_1}, s_2 =$



$H_{\ell_2}, \dots, s_K = H_{\ell_K}$) inside Eq. (2.3) can be further reduced to:

$$\begin{aligned}
& \Pr(\hat{\ell} \neq m | H_m, s_1 = H_{\ell_1}, s_2 = H_{\ell_2}, \dots, s_K = H_{\ell_K}) \\
&= \Pr(\hat{\ell} \neq m | s_1 = H_{\ell_1}, s_2 = H_{\ell_2}, \dots, s_K = H_{\ell_K}) \\
&= \Pr\left(\sum_{k=1}^K \left\| \mathbf{r}_k - \mathbb{P}_{B_k}^{(m)} \mathbf{r}_k \right\|^2 > \min_{1 \leq \ell \leq M} \sum_{k=1}^K \left\| \mathbf{r}_k - \mathbb{P}_{B_k}^{(\ell)} \mathbf{r}_k \right\|^2 \middle| s_1 = H_{\ell_1}, s_2 = H_{\ell_2}, \dots, s_K = H_{\ell_K}\right) \\
&= \Pr\left(\sum_{k=1}^K \left\| \mathbf{r}_k - \mathbb{P}_{B_k}^{(m)} \mathbf{r}_k \right\|^2 > \sum_{k=1}^K \left\| \mathbf{r}_k - \mathbb{P}_{B_k}^{(1)} \mathbf{r}_k \right\|^2 \right. \\
&\quad \text{OR } \sum_{k=1}^K \left\| \mathbf{r}_k - \mathbb{P}_{B_k}^{(m)} \mathbf{r}_k \right\|^2 > \sum_{k=1}^K \left\| \mathbf{r}_k - \mathbb{P}_{B_k}^{(2)} \mathbf{r}_k \right\|^2 \\
&\quad \text{OR } \dots \text{ OR } \sum_{k=1}^K \left\| \mathbf{r}_k - \mathbb{P}_{B_k}^{(m)} \mathbf{r}_k \right\|^2 > \sum_{k=1}^K \left\| \mathbf{r}_k - \mathbb{P}_{B_k}^{(M)} \mathbf{r}_k \right\|^2 \\
&\quad \left. \middle| s_1 = H_{\ell_1}, s_2 = H_{\ell_2}, \dots, s_K = H_{\ell_K}\right) \\
&\leq \sum_{\ell=1, \ell \neq m}^M \Pr\left(\sum_{k=1}^K \left\| \mathbf{r}_k - \mathbb{P}_{B_k}^{(m)} \mathbf{r}_k \right\|^2 > \sum_{k=1}^K \left\| \mathbf{r}_k - \mathbb{P}_{B_k}^{(\ell)} \mathbf{r}_k \right\|^2 \right. \\
&\quad \left. \middle| s_1 = H_{\ell_1}, s_2 = H_{\ell_2}, \dots, s_K = H_{\ell_K}\right)
\end{aligned}$$

where $\mathbf{r}_k = \mathbb{B}_k^{(\ell_k)} \mathbf{h}_k + \mathbf{n}_k$ is the received vector due to the transmission of codeword $\mathbf{b}_k^{(\ell_k)}$.

Thus,

$$\begin{aligned}
& \Pr(\hat{\ell} \neq m | H_m, s_1 = H_{\ell_1}, s_2 = H_{\ell_2}, \dots, s_K = H_{\ell_K}) \\
&\leq \sum_{\ell=1, \ell \neq m}^M \Pr\left(\sum_{k=1}^K \left(\left\| \mathbf{r}_k - \mathbb{P}_{B_k}^{(m)} \mathbf{r}_k \right\|^2 - \left\| \mathbf{r}_k - \mathbb{P}_{B_k}^{(\ell)} \mathbf{r}_k \right\|^2\right) > 0 \right. \\
&\quad \left. \middle| s_1 = H_{\ell_1}, s_2 = H_{\ell_2}, \dots, s_K = H_{\ell_K}\right) \\
&= \sum_{\ell=1, \ell \neq m}^M \Pr\left(\sum_{k=1}^K \mathbf{r}_k^H \left(\mathbb{P}_{B_k}^{(\ell)} - \mathbb{P}_{B_k}^{(m)}\right) \mathbf{r}_k > 0 \middle| s_1 = H_{\ell_1}, s_2 = H_{\ell_2}, \dots, s_K = H_{\ell_K}\right) \quad (2.4)
\end{aligned}$$

Observe that under $s_k = H_{\ell_k}$, the covariance matrix $\mathbb{S}_{\mathbf{r}_k}$ of \mathbf{r}_k is $\mathbb{S}_{\mathbf{r}_k} = \mathbb{B}_k^{(\ell_k)} \mathbb{S}_{\mathbf{h}_k} (\mathbb{B}_k^{(\ell_k)})^T + \sigma_{n_k}^2 \mathbb{I}_L$, where $\mathbb{S}_{\mathbf{h}_k}$ is the covariance matrix of \mathbf{h}_k , and \mathbb{I}_L is the $L \times L$ identity matrix. Then,

by denoting the eigenvalues and eigenvectors of the real and symmetric matrix $\mathbb{S}_{\mathbf{r}_k}^{1/2}(\mathbb{P}_{B_k}^{(\ell)} - \mathbb{P}_{B_k}^{(m)})\mathbb{S}_{\mathbf{r}_k}^{1/2}$ by $\{\lambda_{n,k} = \lambda_{n,k}(\ell, m|\ell_k)\}_{n=1}^L$ and $\{\mathbf{q}_{n,k} = \mathbf{q}_{n,k}(\ell, m|\ell_k)\}_{n=1}^L$ respectively, we have:

$$\mathbb{S}_{\mathbf{r}_k}^{1/2}(\mathbb{P}_{B_k}^{(\ell)} - \mathbb{P}_{B_k}^{(m)})\mathbb{S}_{\mathbf{r}_k}^{1/2} = \sum_{n=1}^L \lambda_{n,k} \mathbf{q}_{n,k} \mathbf{q}_{n,k}^T.$$

It immediately follows that:

$$\begin{aligned} \mathbf{r}_k^H (\mathbb{P}_{B_k}^{(\ell)} - \mathbb{P}_{B_k}^{(m)}) \mathbf{r}_k &= (\mathbb{S}_{\mathbf{r}_k}^{-1/2} \mathbf{r}_k)^H \mathbb{S}_{\mathbf{r}_k}^{1/2} (\mathbb{P}_{B_k}^{(\ell)} - \mathbb{P}_{B_k}^{(m)}) \mathbb{S}_{\mathbf{r}_k}^{1/2} (\mathbb{S}_{\mathbf{r}_k}^{-1/2} \mathbf{r}_k) \\ &= \sum_{n=1}^L \lambda_{n,k} |\mathbf{q}_{n,k}^T \mathbb{S}_{\mathbf{r}_k}^{-1/2} \mathbf{r}_k|^2 \\ &= \sum_{n=1}^L \lambda_{n,k} |X_{n,k}|^2, \end{aligned} \quad (2.5)$$

where

$$X_{n,k} = X_{n,k}(\ell, m|\ell_k) = \mathbf{q}_{n,k}^T \mathbb{S}_{\mathbf{r}_k}^{-1/2} \mathbf{r}_k.$$

Note that under the premise that $\{\mathbf{h}_k\}_{k=1}^K$ and $\{\mathbf{n}_k\}_{k=1}^K$ are independent zero-mean complex Gaussian random vectors with independent components and are independent to each other, $X_{n,k}$ becomes zero-mean complex Gaussian distributed with unit variance, and is independent for different n and k , which implies that $\{|X_{n,k}|^2\}_{1 \leq n \leq L, 1 \leq k \leq K}$ are independent χ^2 -distributed with two degree of freedom.

To continue the derivation, we assume without loss of generality that:

1. there are \bar{L} different non-zero eigenvalues in $\{\lambda_{n,k}\}_{1 \leq n \leq L, 1 \leq k \leq K}$, denoted by $\{\bar{\lambda}_\ell\}_{\ell=1}^{\bar{L}}$ with $\bar{\lambda}_1 > \bar{\lambda}_2 > \dots > \bar{\lambda}_{\bar{L}}$;
2. the individual orders of multiplicity of $\{\bar{\lambda}_\ell\}_{\ell=1}^{\bar{L}}$ are $\{k_\ell\}_{\ell=1}^{\bar{L}}$.

As a result, the sum of (2.5) can be rewritten as:

$$\begin{aligned} \sum_{k=1}^K \mathbf{r}_k^H (\mathbb{P}_{B_k}^{(\ell)} - \mathbb{P}_{B_k}^{(m)}) \mathbf{r}_k &= \sum_{k=1}^K \sum_{n=1}^L \lambda_{n,k} |X_{n,k}|^2 \\ &= \sum_{\ell=1}^{\bar{L}} \bar{\lambda}_\ell \cdot \chi^2(2k_\ell), \end{aligned}$$

where $\chi^2(2k)$ is χ^2 -distributed with $2k$ degree of freedom, and

$$E \left[\exp \left\{ jt \sum_{k=1}^K \mathbf{r}_k^H (\mathbb{P}_{B_k}^{(\ell)} - \mathbb{P}_{B_k}^{(m)}) \mathbf{r}_k \right\} \right] = \prod_{n=1}^{\bar{L}} (1 - 2j\bar{\lambda}_n t)^{-k_n/2}, \quad (2.6)$$

where j denotes the imaginary part. Resume the derivation in (2.5):

$$\begin{aligned} & \Pr(\hat{\ell} \neq m | H_m, s_1 = H_{\ell_1}, s_2 = H_{\ell_2}, \dots, s_K = H_{\ell_K}) \\ & \leq \sum_{\ell=1, \ell \neq m}^M \Pr \left(\sum_{k=1}^K \mathbf{r}_k^H (\mathbb{P}_{B_k}^{(\ell)} - \mathbb{P}_{B_k}^{(m)}) \mathbf{r}_k > 0 \middle| s_1 = H_{\ell_1}, s_2 = H_{\ell_2}, \dots, s_K = H_{\ell_K} \right) \\ & = \sum_{\ell=1, \ell \neq m}^M \frac{1}{2\pi} \int_0^\infty \left(\int_{-\infty}^\infty \prod_{n=1}^{\bar{L}} (1 - 2j\bar{\lambda}_n t)^{-k_n/2} e^{-jtr} dt \right) dr. \end{aligned} \quad (2.7)$$

Note again that $\{\bar{\lambda}_n = \bar{\lambda}_n(\ell, m)\}_{n=1}^{\bar{L}}$ is a function of ℓ, m and

$$\mathbf{s} = \begin{bmatrix} s_1 \\ s_2 \\ \vdots \\ s_K \end{bmatrix}.$$

In the special case of Rayleigh fading channels, where $\{\mathbf{h}_k\}_{k=1}^K$ are assumed zero-mean Gaussian distributed, (2.7) can be further derived as [7]:

$$\begin{aligned} & \Pr(\hat{\ell} \neq m | H_m, s_1 = H_{\ell_1}, s_2 = H_{\ell_2}, \dots, s_K = H_{\ell_K}) \\ & \leq \sum_{\ell=1, \ell \neq m}^M \frac{1}{2\pi} \int_0^\infty \left(\int_{-\infty}^\infty \prod_{n=1}^{\bar{L}} (1 - 2j\bar{\lambda}_n t)^{-k_n/2} e^{-jtr} dt \right) dr \\ & = \sum_{\ell=1, \ell \neq m}^M \sum_{n=1}^{\bar{L}} \frac{1}{(k_n - 1)!} \left[\frac{\partial^{(k_n-1)}}{\partial x^{(k_n-1)}} F_n(x) \right]_{x=\bar{\lambda}_n}, \end{aligned}$$

where

$$F_n(x) = x^{\sum_{i=1}^{\bar{L}} k_i - 1} \prod_{u=1, u \neq n}^{\bar{L}} (x - \bar{\lambda}_u)^{-k_u}.$$

We finally conclude:

$$P_e \leq \sum_{m=1}^M \Pr(H_m) \sum_{\ell_1=1}^M \sum_{\ell_2=1}^M \dots \sum_{\ell_K=1}^M P_{\ell_1|m}^{(1)} P_{\ell_2|m}^{(2)} \dots P_{\ell_K|m}^{(K)} \sum_{\ell=1, \ell \neq m}^M \sum_{n=1}^{\bar{L}} \frac{1}{(k_n - 1)!} \left[\frac{\partial^{(k_n-1)}}{\partial x^{(k_n-1)}} F_n(x) \right]_{x=\bar{\lambda}_n}. \quad (2.8)$$

2.2.1 Union Bound Under Rayleigh Fadings With Perfect Sensor Observations

By adding the perfect-sensor-observation assumption that $P_{\ell|m}^{(i)} = 1$ when $\ell = m$, (2.8) reduces to:

$$P_e \leq \sum_{m=1}^M \Pr(H_m) \sum_{\ell=1, \ell \neq m}^M \sum_{n=1}^{\bar{L}} \frac{1}{(k_n - 1)!} \left[\frac{\partial^{(k_n-1)}}{\partial x^{(k_n-1)}} F_n(x) \right]_{x=\bar{\lambda}_n}, \quad (2.9)$$

where $\{\bar{\lambda}_n\}_{n=1}^{\bar{L}}$ are now only dependent on ℓ and m , and the local decisions always equal

$$\mathbf{s} = \begin{bmatrix} s_1 \\ s_2 \\ \vdots \\ s_K \end{bmatrix} = \begin{bmatrix} H_m \\ H_m \\ \vdots \\ H_m \end{bmatrix}.$$

2.2.2 Union Bound Under Rayleigh Fadings With Faulty Sensors

In this section, we rederive the union bound under Rayleigh fadings with faulty sensors as similarly to the previous two sections. For simplicity, we assume that the first sensor is faulty, namely $\mathbf{b}_1 = \mathbf{c}$ is nothing to do with the local observation and the true hypothesis.

Again, we begin with:

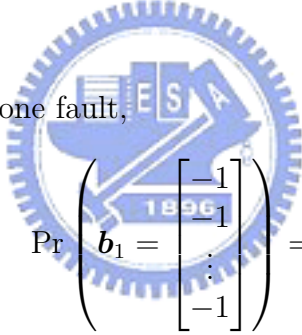
$$P_e = \sum_{m=1}^M \Pr(H_m) \Pr(\hat{\ell} \neq m | H_m)$$

Then, denoting by s_i the local decision at sensor i , we obtain:

$$\begin{aligned}
& \Pr(\hat{\ell} \neq m | H_m) \\
&= \sum_{\mathbf{c} \in \{\pm 1\}^N} \sum_{\ell_2=1}^M \sum_{\ell_3=1}^M \cdots \sum_{\ell_K=1}^M \Pr(\hat{\ell} \neq m | H_m, \mathbf{b}_1 = \mathbf{c}, s_2 = H_{\ell_2}, \dots, s_K = H_{\ell_K}) \\
&\quad \times \Pr(\mathbf{b}_1 = \mathbf{c}, s_2 = H_{\ell_2}, \dots, s_K = H_{\ell_K} | H_m) \\
&= \sum_{\mathbf{c} \in \{\pm 1\}^N} \sum_{\ell_2=1}^M \sum_{\ell_3=1}^M \cdots \sum_{\ell_K=1}^M \Pr(\hat{\ell} \neq m | H_m, \mathbf{b}_1 = \mathbf{c}, s_2 = H_{\ell_2}, \dots, s_K = H_{\ell_K}) \\
&\quad \times \Pr(\mathbf{b}_1 = \mathbf{c}) \Pr(s_2 = H_{\ell_2} | H_m) \cdots \Pr(s_K = H_{\ell_K} | H_m) \\
&= \sum_{\mathbf{c} \in \{\pm 1\}^N} \sum_{\ell_2=1}^M \sum_{\ell_3=1}^M \cdots \sum_{\ell_K=1}^M \Pr(\hat{\ell} \neq m | H_m, \mathbf{b}_1 = \mathbf{c}, s_2 = H_{\ell_2}, \dots, s_K = H_{\ell_K}) \\
&\quad \times \Pr(\mathbf{b}_1 = \mathbf{c}) P_{\ell_2|m}^{(2)} \cdots P_{\ell_K|m}^{(K)}. \tag{2.10}
\end{aligned}$$

Hence, all the procedures of the previous two sections follow except that $P_{\ell_1|m}^{(1)}$ is replaced by $\Pr(\mathbf{b}_1 = \mathbf{c})$.

As an example, for stuck-at-one fault,



$$\Pr \left(\mathbf{b}_1 = \begin{bmatrix} -1 \\ -1 \\ \vdots \\ -1 \end{bmatrix} \right) = 1.$$

For random fault,

$$\Pr(\mathbf{b}_1 = \mathbf{c}) = \frac{1}{2^N}$$

for every $\mathbf{c} \in \{\pm 1\}^N$.

2.3 Code Search

Simulated annealing [8] is a popular algorithm for finding the optimum solution of certain problems. It mimics a physical phenomenon about temperature control. Specifically, a system containing high entropy at high temperature is set at the beginning. Then, the

system temperature is cooled down gradually at each iteration until a stable solution at low temperature is reached.

Here, we employ the simulated annealing algorithm to find the optimum codebook in our wireless sensor network system. The error probability bound in (2.8) is regarded as the system entropy. In other words, the codebook has high error probability bound value when the temperature is high. During the procedure, the error probability bound is supposed to be cooled down until the target codebook is found.

In order to further simplify the code search process, we found that the bound in (2.4) (equivalently, (2.11)) can be further upper-bounded by:

$$\begin{aligned}
& \Pr(\hat{\ell} \neq m | H_m, s_1 = H_{\ell_1}, s_2 = H_{\ell_2}, \dots, s_K = H_{\ell_K}) \\
& \leq \sum_{\ell=1, \ell \neq m}^M \Pr \left(\sum_{k=1}^K \mathbf{r}_k^H \left(\mathbb{P}_{B_k}^{(\ell)} - \mathbb{P}_{B_k}^{(m)} \right) \mathbf{r}_k > 0 \middle| s_1 = H_{\ell_1}, s_2 = H_{\ell_2}, \dots, s_K = H_{\ell_K} \right) \quad (2.11) \\
& \leq \sum_{\ell=1, \ell \neq m}^M \sum_{k=1}^K \Pr \left(\mathbf{r}_k^H \left(\mathbb{P}_{B_k}^{(\ell)} - \mathbb{P}_{B_k}^{(m)} \right) \mathbf{r}_k > 0 \middle| s_1 = H_{\ell_1}, s_2 = H_{\ell_2}, \dots, s_K = H_{\ell_K} \right) \\
& = \sum_{\ell=1, \ell \neq m}^M \sum_{k=1}^K \Pr \left(\mathbf{r}_k^H \left(\mathbb{P}_{B_k}^{(\ell)} - \mathbb{P}_{B_k}^{(m)} \right) \mathbf{r}_k > 0 \middle| s_k = H_{\ell_k} \right). \quad (2.12)
\end{aligned}$$

Equation (2.12), when it is regarded as an alternative entropy function for simulated annealing, then indicates that the sub-codebook for each sensor can be searched separately, thereby greatly reducing the complexity for codebook search. Our simulates showed that in those cases we considered, the resultant codebook by minimizing the global criterion (2.11) is almost no different from that by minimizing (2.12). As an example, Figure 2.2 shows that for sixty different codes tested, the two bounds, i.e. (2.11) and (2.12), have the same trend in their quantities, which confirmed that the code that minimizes either (2.11) or (2.12) should be the same among these sixty randomly chosen codes. Figure 2.3 indicates that under two sensors, codeword length $N = 5$ and two hypothesis (abbreviated as S2N5H2 in the title of the figure), the best code that minimizes (2.12) performs almost the same as the one that

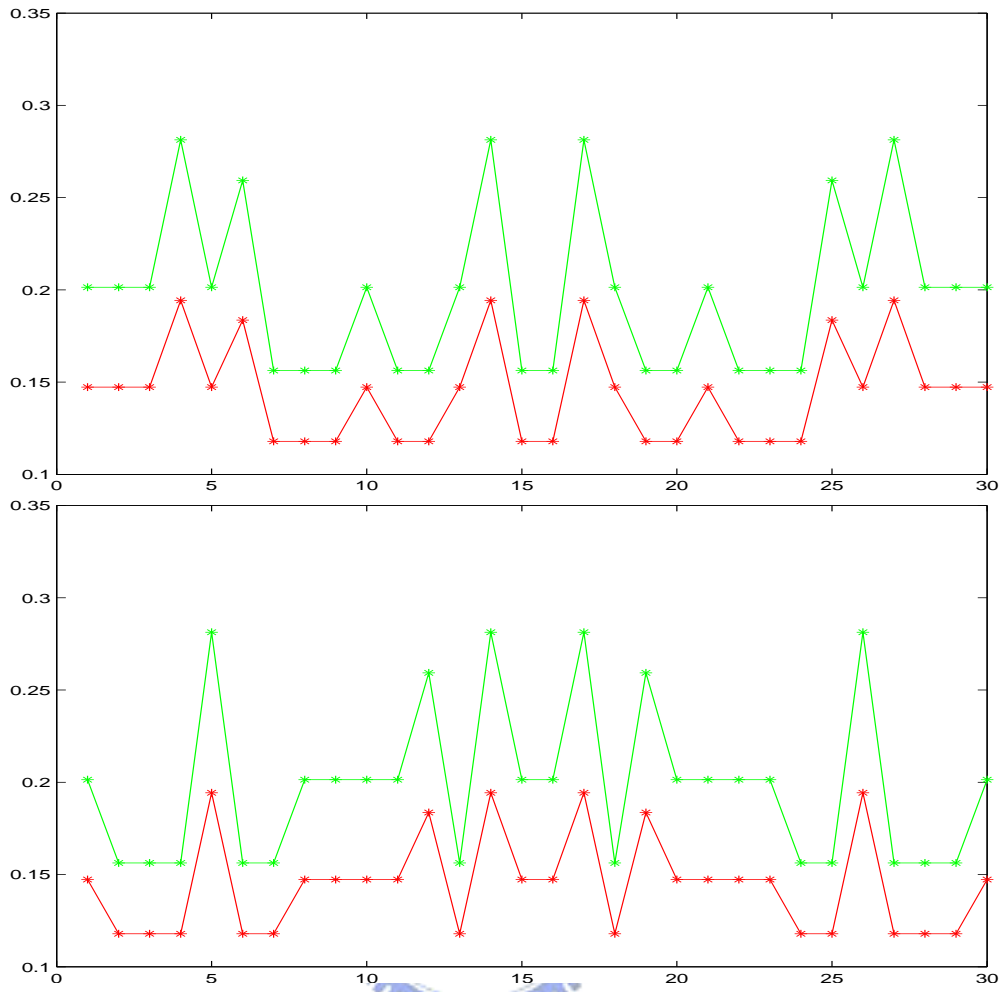


Figure 2.2: The bounds in (2.11) (red points) and (2.12) (green points) for sixty different codes.

minimizes (2.11).

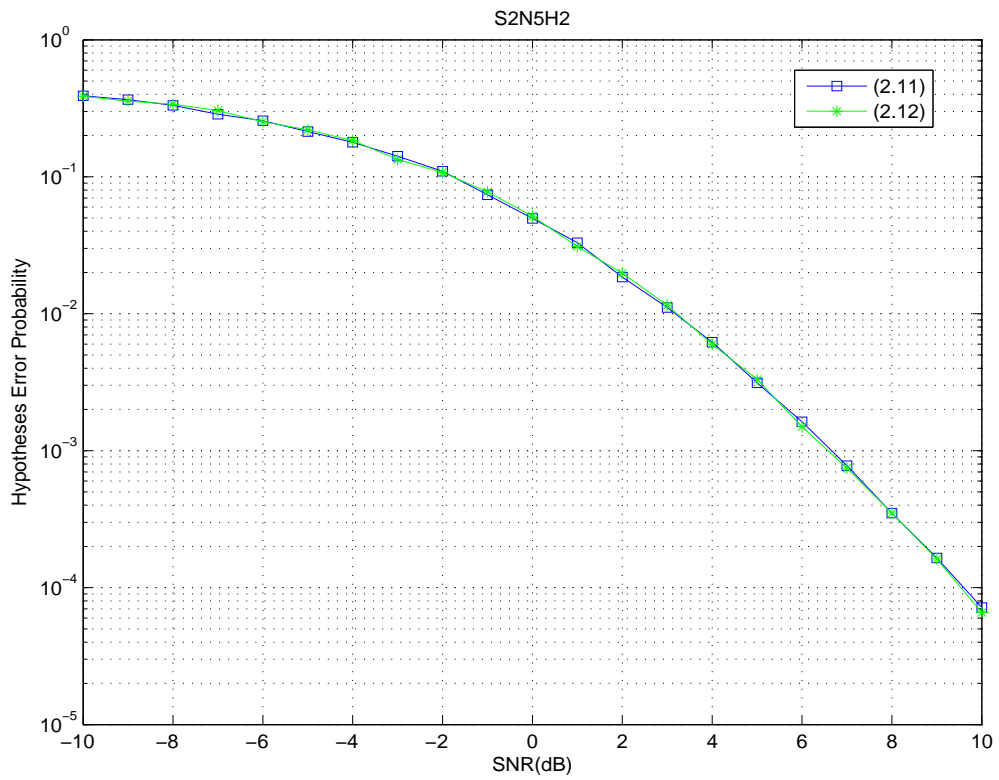


Figure 2.3: Performances of the best codes searched in terms of different union bound criterions.

Chapter 3

Simulation Results

In this chapter, we will examine the performance of the design that combines channel estimation and sensor fault protection in wireless sensor network. The channel coefficients \mathbf{h}_i in the wireless link between sensor i and the fusion center is assumed to be independently and identically zero-mean complex Gaussian distributed with memory order $(P - 1) = 1$ and $E[|h_{i,1}|^2] = E[|h_{i,2}|^2] = 1/2$, and $\{\mathbf{h}_i\}_{i=1}^K$ are also independent across sensors. The prior probability for each hypothesis is assumed equal. The operating signal-to-noise ratio (SNR) for the codeword search introduced in Section 2.3 is set to be 10 dB. Since

$$\mathbb{P}_B = \mathbb{B}[\mathbb{B}^T \mathbb{B}]^{-1} \mathbb{B}^T = (-\mathbb{B})[(-\mathbb{B})^T (-\mathbb{B})]^{-1} (-\mathbb{B})^T = \mathbb{P}_{-B},$$

the fusion center cannot differentiate the transmissions between \mathbf{b} and $-\mathbf{b}$. For this reason, we will fix b_1 as -1 in the code design. Finally, when sensor faults occur, we assume that the fusion center is unaware of which one is out of control.

3.1 Parameter Determination for Least Square (LS) Estimation

Based upon the channel model in Chapter 2.1, namely,

$$\mathbb{R} = [\mathbf{r}_1 \quad \mathbf{r}_2 \quad \cdots \quad \mathbf{r}_K] = [\mathbb{B}_1 \mathbf{h}_1 \quad \mathbb{B}_2 \mathbf{h}_2 \quad \cdots \quad \mathbb{B}_K \mathbf{h}_K] + \mathbb{N},$$

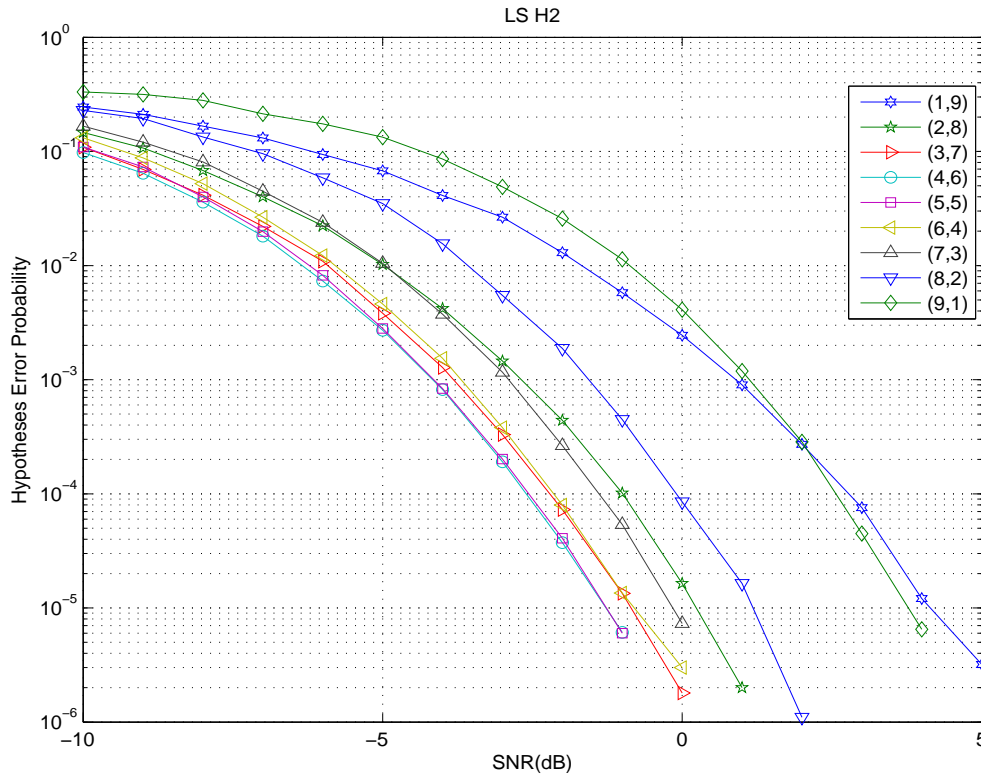


Figure 3.1: Performances of hypothesis detection based on LS estimate of channel coefficients in terms of training sequences. Ten sensors, each transmitting ten bits, and two hypotheses are assumed. In the legend, $LS(x,y)$ represents that x training bits and y code bits are transmitted.

where \mathbb{N} are white and Gaussian, we obtain that for known training sequences \mathbb{B}_k at sensor k , the least square (LS) estimate of the channel coefficients are given by [11]:

$$\hat{\mathbf{h}}_k = (\mathbb{B}_k^T \mathbb{B}_k)^{-1} \mathbb{B}_k^T \mathbf{r}_k$$

We can then use the estimate channel coefficients to determine the hypothesis as:

$$\hat{\ell} = \arg \min_{\{H_\ell\}} \sum_{k=1}^K \left\| \mathbf{r}_k - \mathbb{B}_k^{(\ell)} \mathbf{h}_k \right\|^2.$$

Figure 3.1 summarizes the simulations for different ratio of training bits subject to fixed transmission length of 10 bits per sensor. The codewords for two hypotheses are respectively all-negative-one and all-positive-one sequences. The training sequence is taken to be all-negative-one. Our result indicates that the choice of four training bits, followed by six information bits, results in the best performance. We will accordingly adopt this ratio when the hypothesis-detection-based-on-LS-channel-estimate scheme (hereafter, abbreviated as the LSE scheme) is compared with the combined-channel-estimation-and-sensor-fault-protection scheme (hereafter, abbreviated as the COM scheme).

Throughout this chapter, “LS” in the legend of the figure will be reserved to denote the hypothesis-detection-based-on-LS-channel-estimate scheme except otherwise stated. Specifically, “LS(x, y)” represents the hypothesis-detection-based-on-LS-channel-estimate scheme with x training bits and y code bits. In addition, “Nx”, “Sy” and “Hz” (either in the figure title or in the figure legend) will respectively denote “ x bits transmitted per sensor”, “ y sensors” and “ z hypotheses”.

3.2 Deep Fade Effect Due to Soft-Decision

Figures 3.2–3.9 summarizes the comparison of the hypothesis detection error probabilities for the LSE and the COM schemes. These results indicate that in fault-free situation, the

COM scheme always perform better than the respective equal-length LSE scheme, when the total number of transmitted bits (i.e., the product of the sensor number, S , and the number of the transmitted bits per sensor, N) is less than 100. Further growth of $S \times N$ up to 100 will induce a sudden performance degradation at $\text{SNR} = -9$ dB for the COM scheme such as S5H2:N20 in Fig. 3.3. We then notice that the SNR break points of the sudden performance degradation for the COM scheme will increase as $S \times N$ grows (cf. Table 3.1). An interpretation of this sudden performance degradation is that in absence of channel estimation and equalization, the soft-decision based on the criterion of

$$\hat{\ell} = \arg \min_{1 \leq \ell \leq M} \sum_{k=1}^K \left\| \mathbf{r}_k - \mathbb{P}_{B_k}^{(\ell)} \mathbf{r}_k \right\|^2 \quad (3.1)$$

may suffer the so-called “deep fading” effect, under which the correct codeword may be removed simply because its accumulated metric $\sum_{k=1}^K \left\| \mathbf{r}_k - \mathbb{P}_{B_k}^{(\ell)} \mathbf{r}_k \right\|^2$ is slightly worse than that of some other codeword by few unexpected deep fading. The more the total number of the transmitted bits, the higher the probability that the deep fading occurs. This explains the reason why the SNR break points of the sudden performance degradation become larger when $S \times N$ increases.

Figures 3.10–3.13 also confirm our interpretation on sudden performance degradation of the soft-decision COM scheme. By employing hard-decision, where $\{\mathbf{r}_k\}_{k=1}^K$ is first binary-quantized into $\{\pm 1\}$ before taking into (3.1), the sudden performance degradation of the COM scheme disappears as anticipated, and therefore, the hard-decision COM scheme always outperforms the equal-length hard-decision LSE scheme.

Next, we re-perform the simulations in Figs. 3.2–3.9 by introducing one faulty sensor, and summarize them in Figs. 3.14–3.21. The COM schemes again outperform the LSE schemes except for the sudden performance degradation due to deep fading effect. The SNR break points at each figure remains exactly the same. In addition, an error floor phenomenon for the COM scheme appears due to that the fusion center is unaware of which sensor is faulty.

Table 3.1: The SNRs corresponding to sudden performance degradation of the COM scheme.

S	5	10	8	5	10	8	8	10	10
N	20	10	15	25	15	20	25	20	25
$S \times N$	100	100	120	125	150	160	200	200	250
Sudden degraded SNR break point (dB)	-9	-9	-8	-8	-7	-7	-6	-6	-5
See Fig.	3.3	3.5	3.4	3.3	3.5	3.4	3.4	3.5	3.5
Also see Fig.	3.8	3.6	3.7	3.9	3.7	3.8	3.9	3.8	3.9

Since the LSE scheme can detect the faulty sensor by means of the training sequence, the fusion can exclude those untrustworthy receptions, and hence, no error floor occurs in their performance curves.

In Figs. 3.22-3.25, we refine the LSE schemes as the fusion only uses the training bits to do channel estimation, and no detection of faulty sensors is conducted. As anticipated, the error floors appear as well for the LSE schemes. Yet, because the information-bearing bits of the LSE schemes are shorter than those of the COM schemes, the error floor level of the LSE schemes is considerably higher than the respective COM schemes. This results hint that without the faulty sensor detection, the COM schemes are indeed more robust at medium-to-high SNRs.

According to Figs. 3.26-3.29, by ignoring the sudden performance degradation at low SNRs and the error flooring at high SNRs, the COM schemes survive 20% sensor faulty ratio when they are compared with the LSE schemes.

Figures 3.30–3.49 repeats the previous simulations with four hypotheses. Since the results show basically the same behaviors, their remarks are omitted.

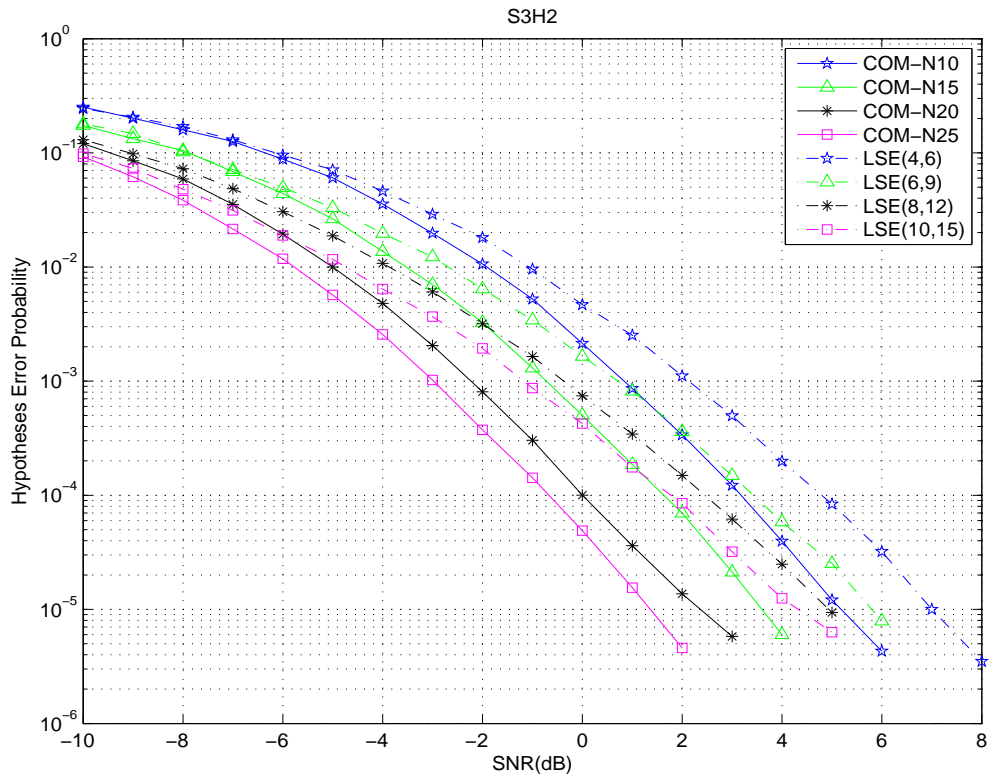


Figure 3.2: Performances of hypothesis detection. “S3H2” represents three sensors and two hypotheses are assumed in this figure.

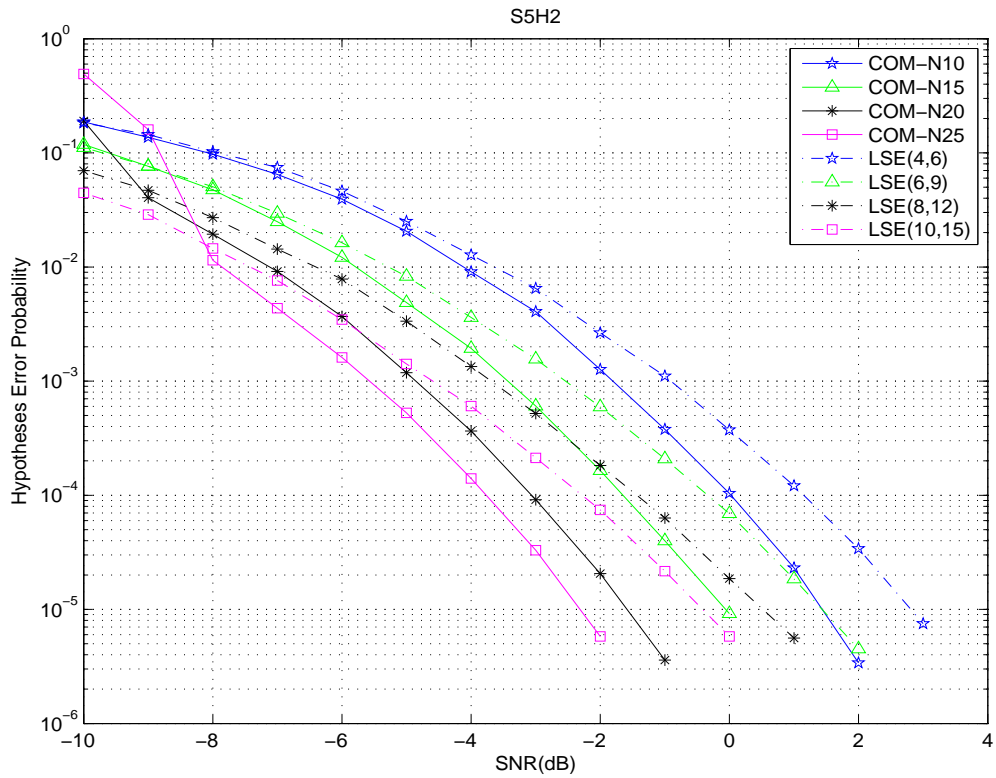


Figure 3.3: Performances of hypothesis detection. “S5H2” represents five sensors and two hypotheses are assumed in this figure.

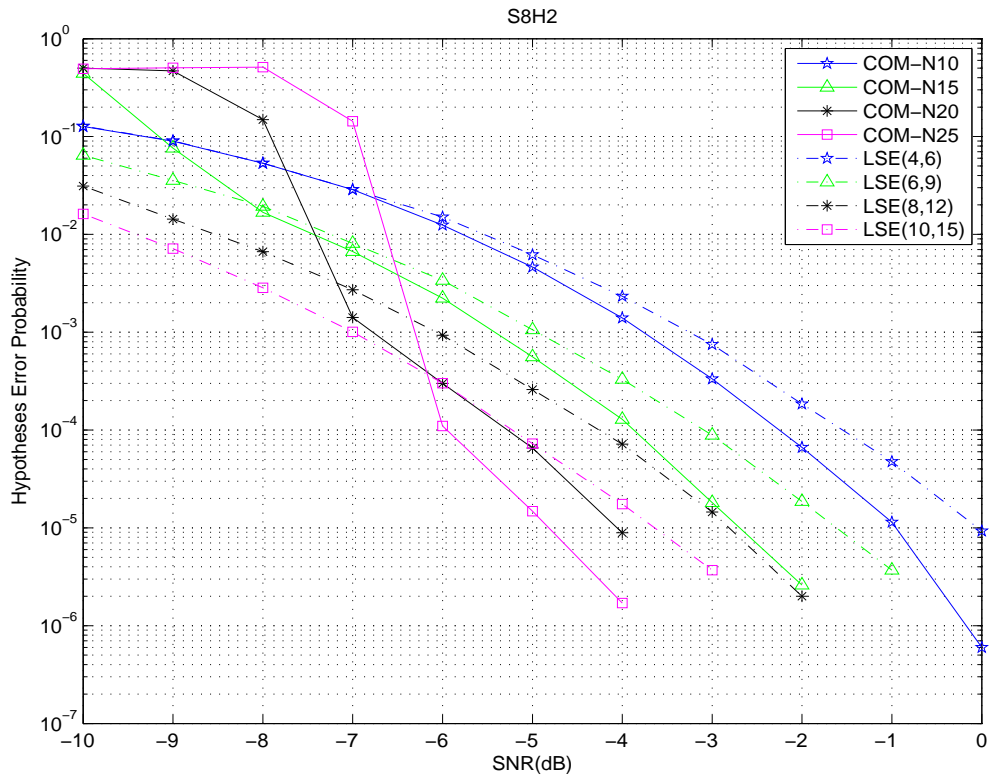


Figure 3.4: Performances of hypothesis detection. “S8H2” represents eight sensors and two hypotheses are assumed in this figure.

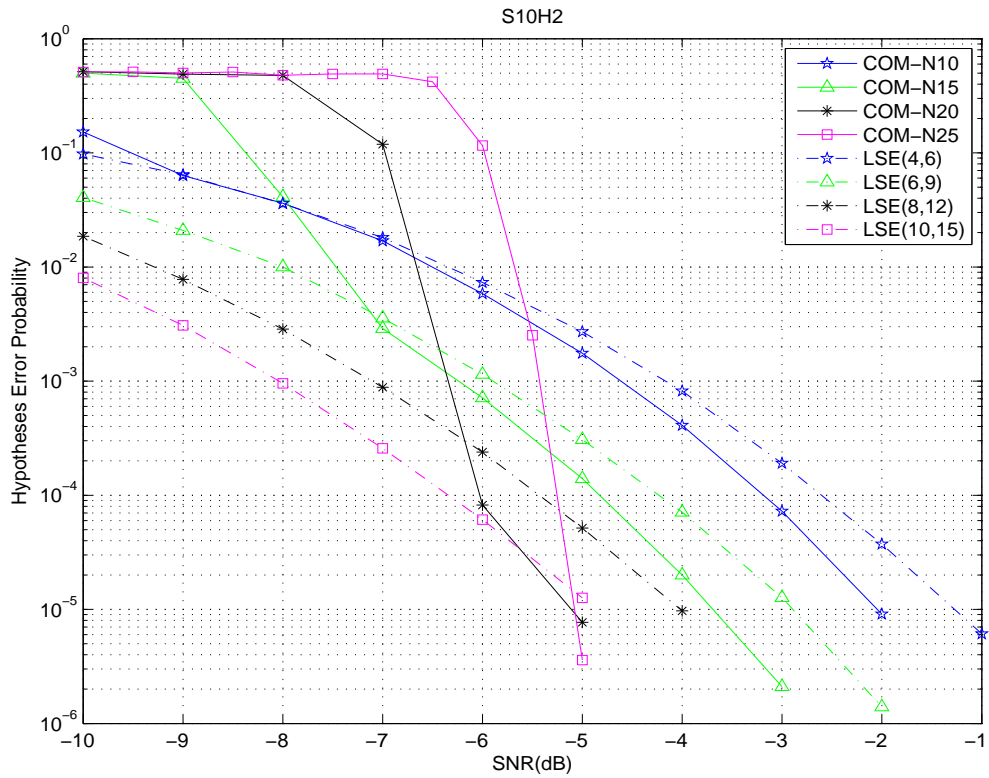


Figure 3.5: Performances of hypothesis detection. “S10H2” represents ten sensors and two hypotheses are assumed in this figure.

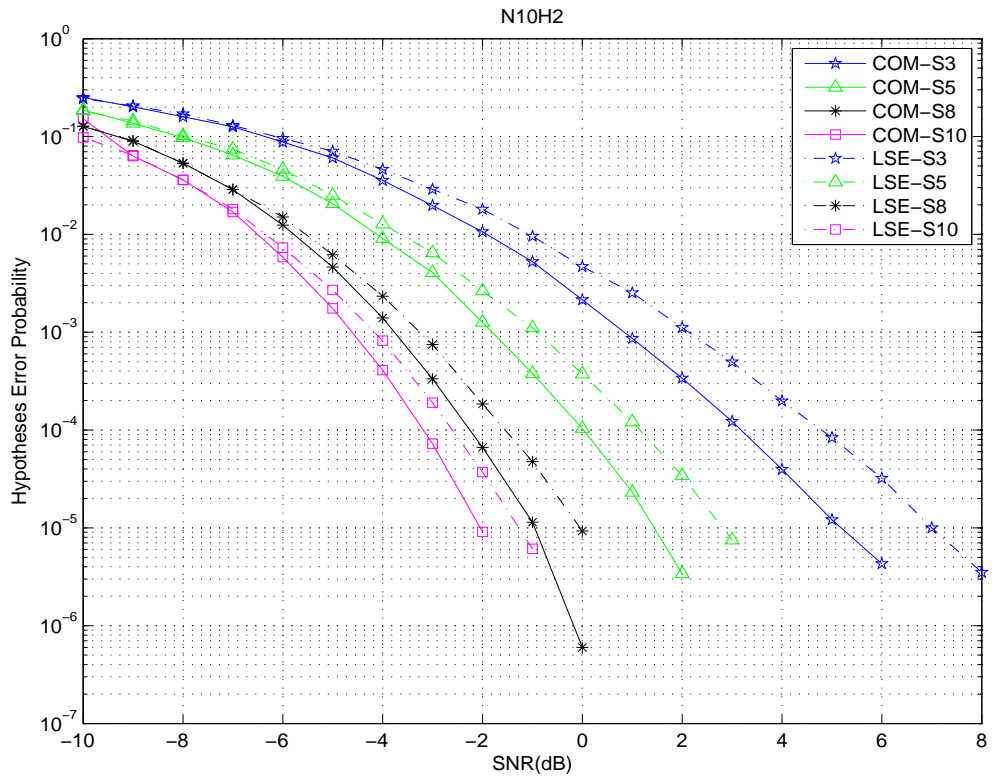


Figure 3.6: Performances of hypothesis detection. “N10H2” represents 10 bits per sensor and two hypotheses are assumed in this figure.

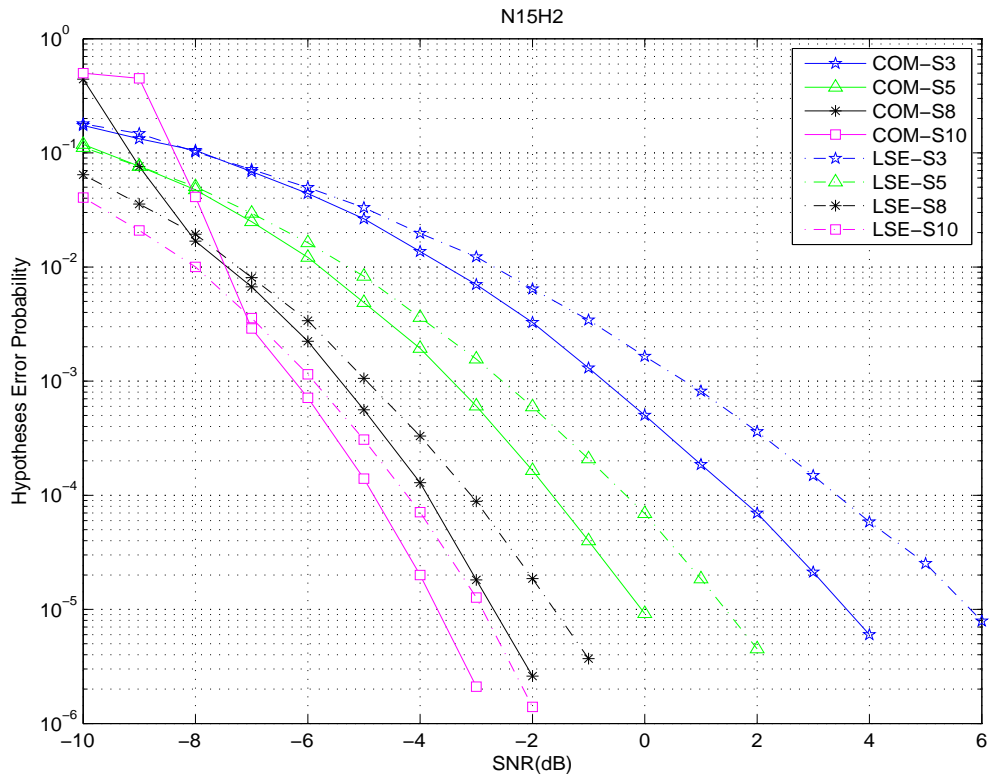


Figure 3.7: Performances of hypothesis detection. “N15H2” represents 15 bits per sensor and two hypotheses are assumed in this figure.

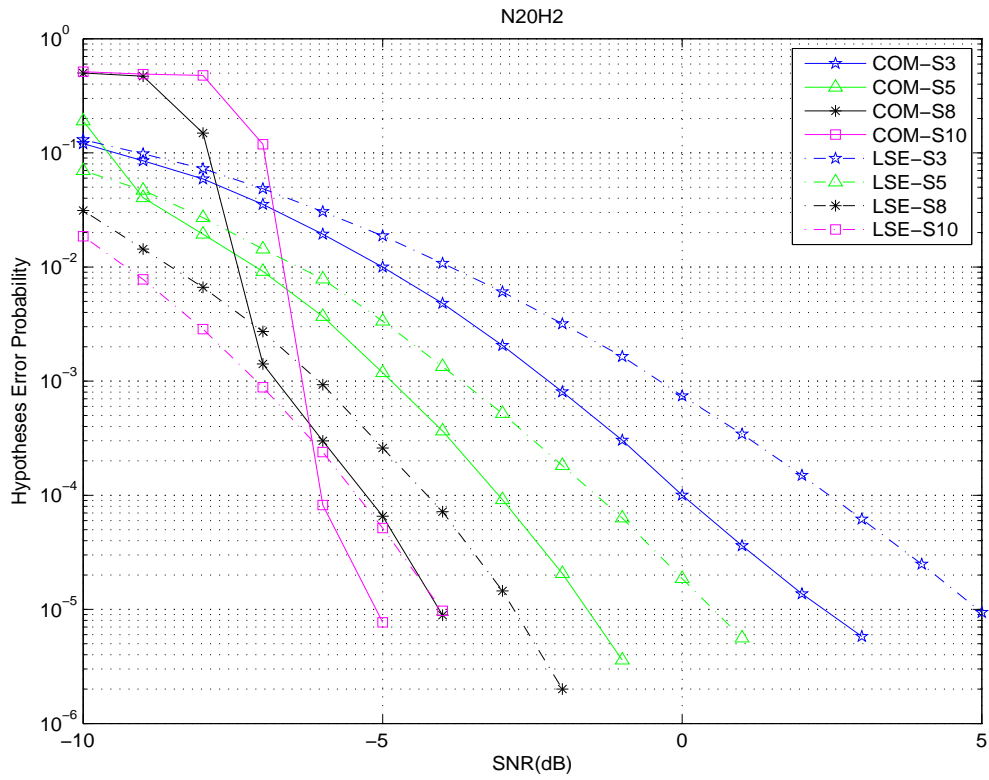


Figure 3.8: Performances of hypothesis detection. “N20H2” represents 20 bits per sensor and two hypotheses are assumed in this figure.

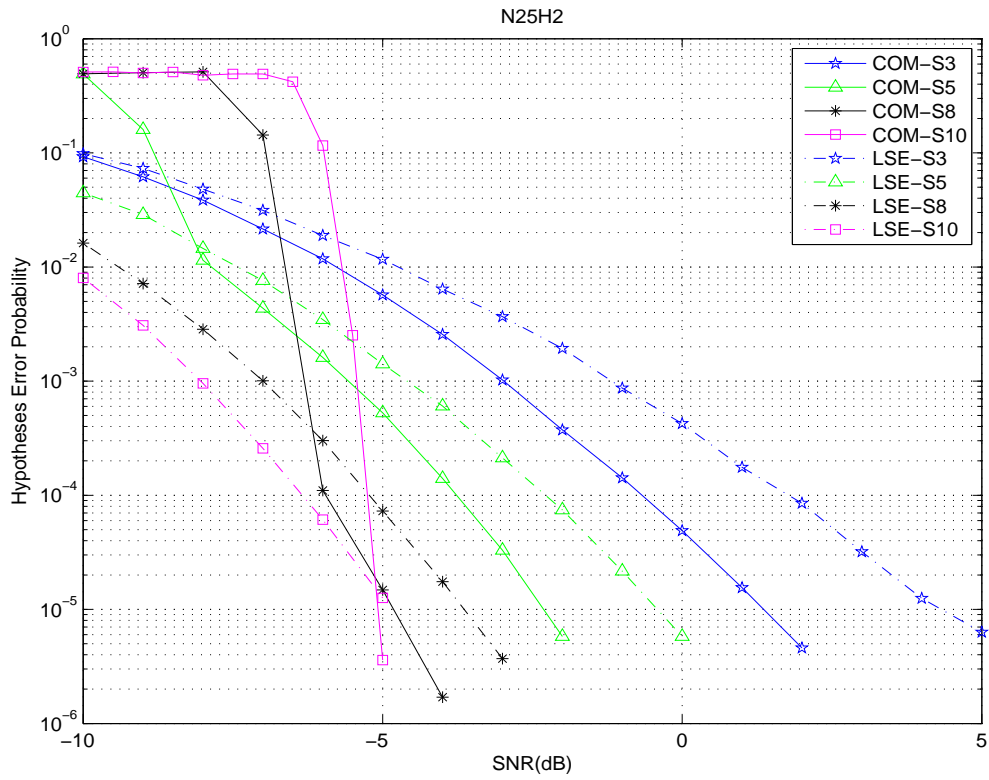


Figure 3.9: Performances of hypothesis detection. “N25H2” represents 25 bits per sensor and two hypotheses are assumed in this figure.

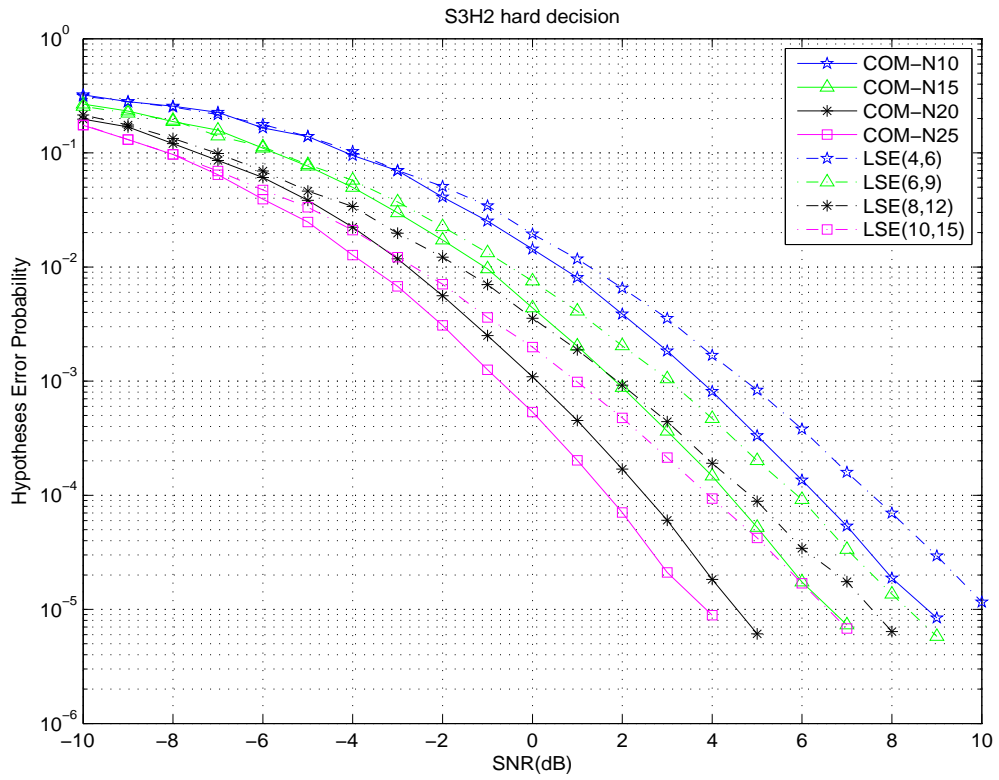


Figure 3.10: Performances of hypothesis detection. “S3H2 hard decision” represents three sensors, two hypotheses, hard-decision fusion are assumed in this figure.

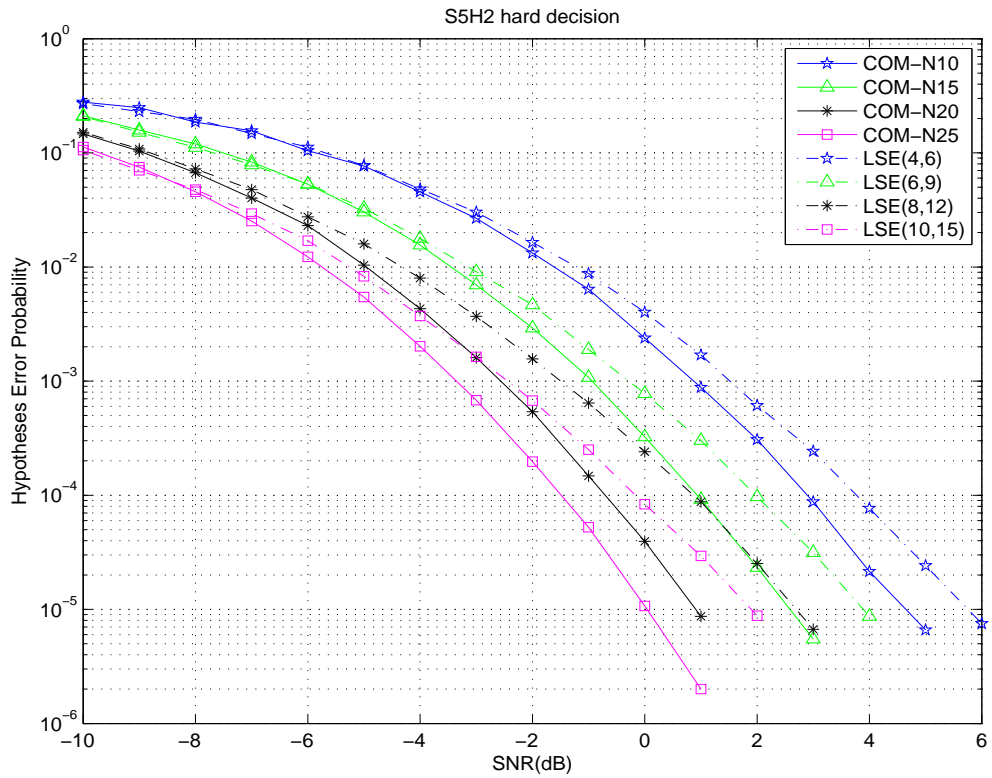


Figure 3.11: Performances of hypothesis detection. “S5H2 hard decision” represents five sensors, two hypotheses, hard-decision fusion are assumed in this figure.

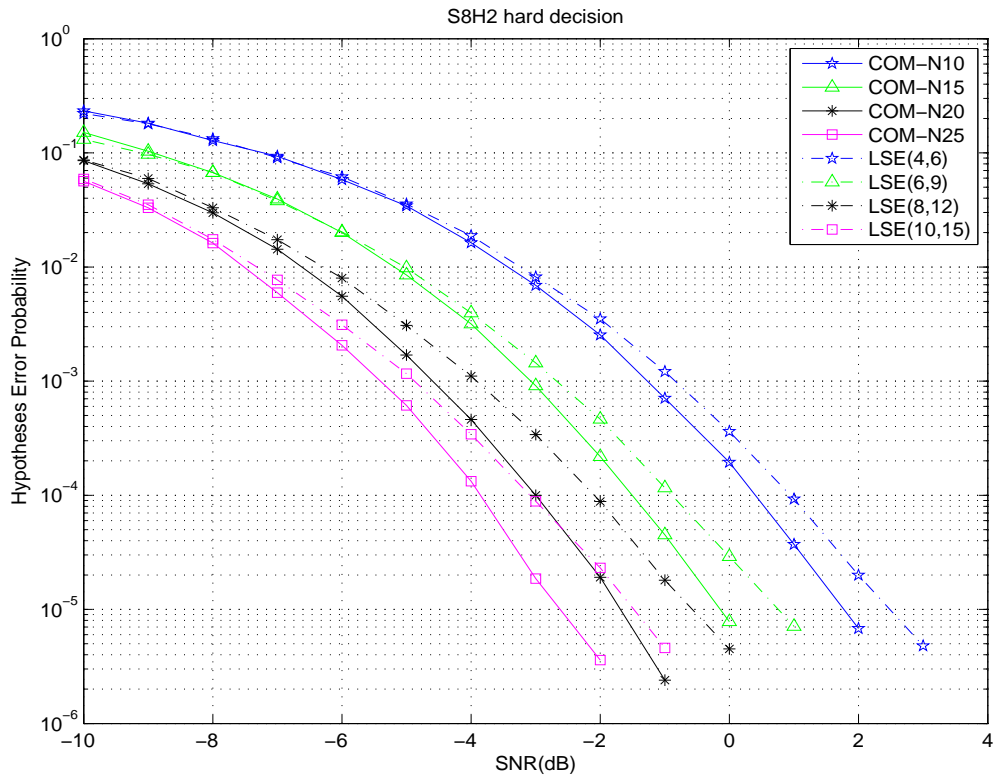


Figure 3.12: Performances of hypothesis detection. “S8H2 hard decision” represents eight sensors, two hypotheses, hard-decision fusion are assumed in this figure.

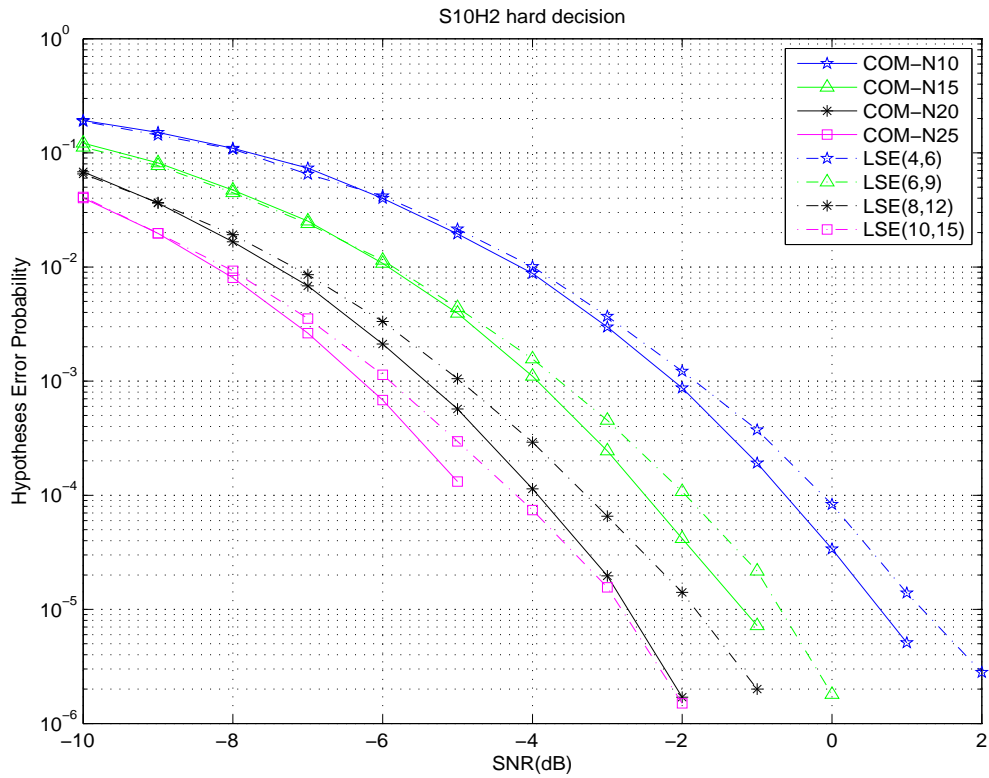


Figure 3.13: Performances of hypothesis detection. “S10H2 hard decision” represents ten sensors, two hypotheses, hard-decision fusion are assumed in this figure.

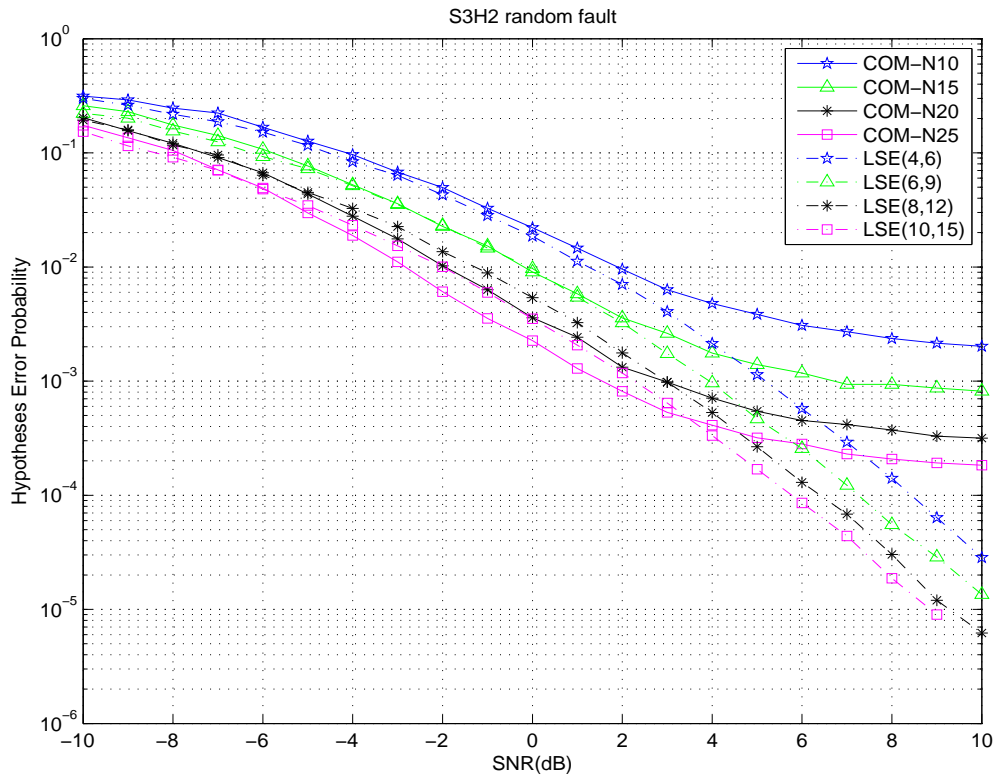


Figure 3.14: Performance of hypothesis detection. “S3H2 random fault” represents three sensors, two hypotheses and one random faulty sensor are assumed in this figure.

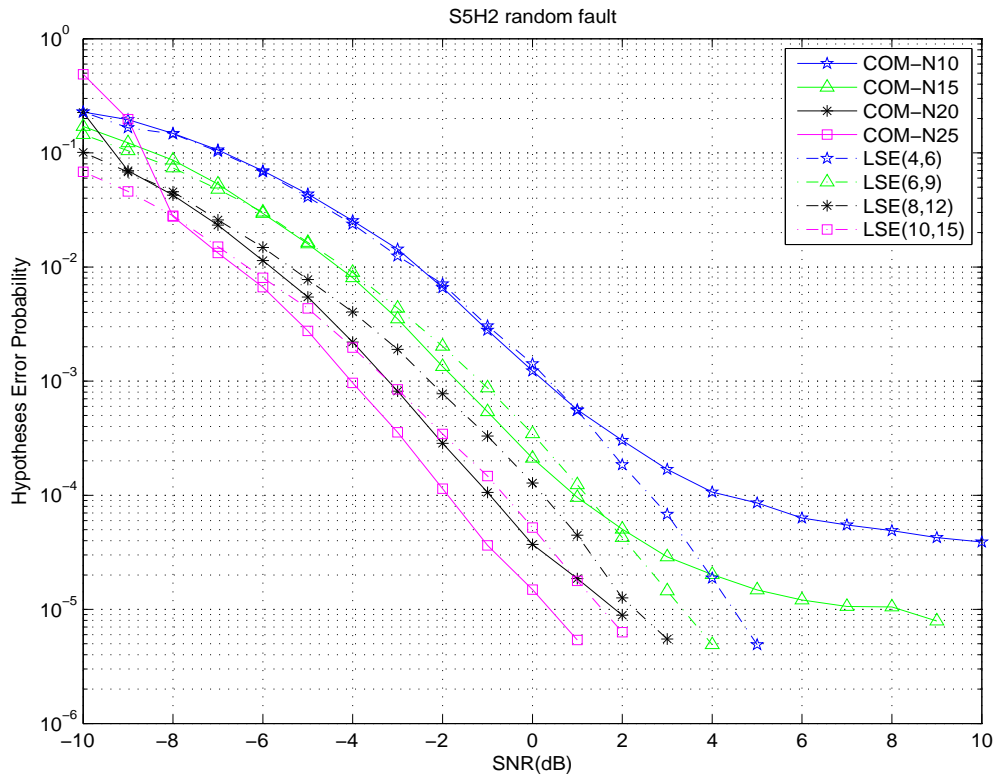


Figure 3.15: Performance of hypothesis detection. “S5H2 random fault” represents five sensors, two hypotheses and one random faulty sensor are assumed in this figure.

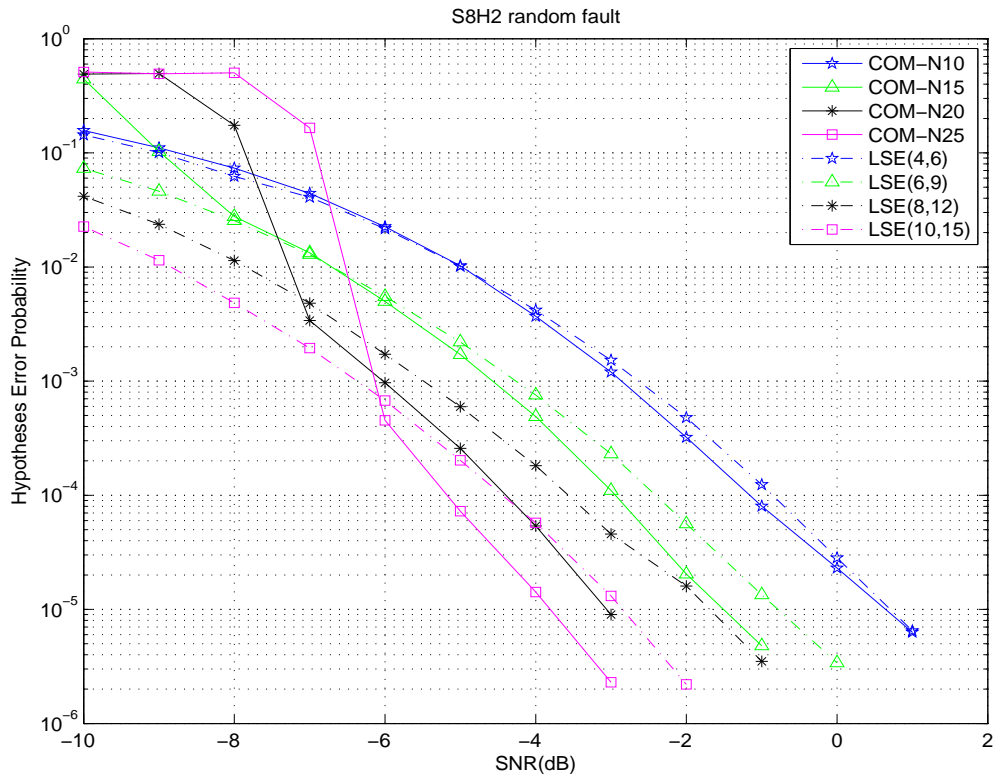


Figure 3.16: Performance of hypothesis detection. “S8H2 random fault” represents eight sensors, two hypotheses and one random faulty sensor are assumed in this figure.

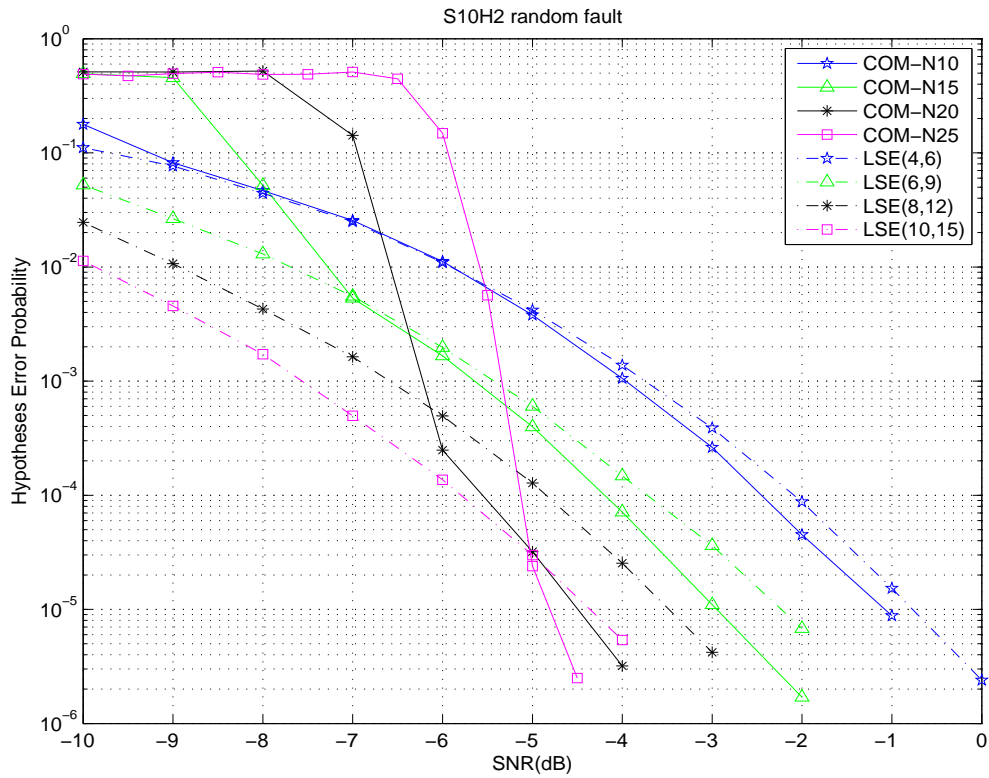


Figure 3.17: Performance of hypothesis detection. “S10H2 random fault” represents ten sensors, two hypotheses and one random faulty sensor are assumed in this figure.

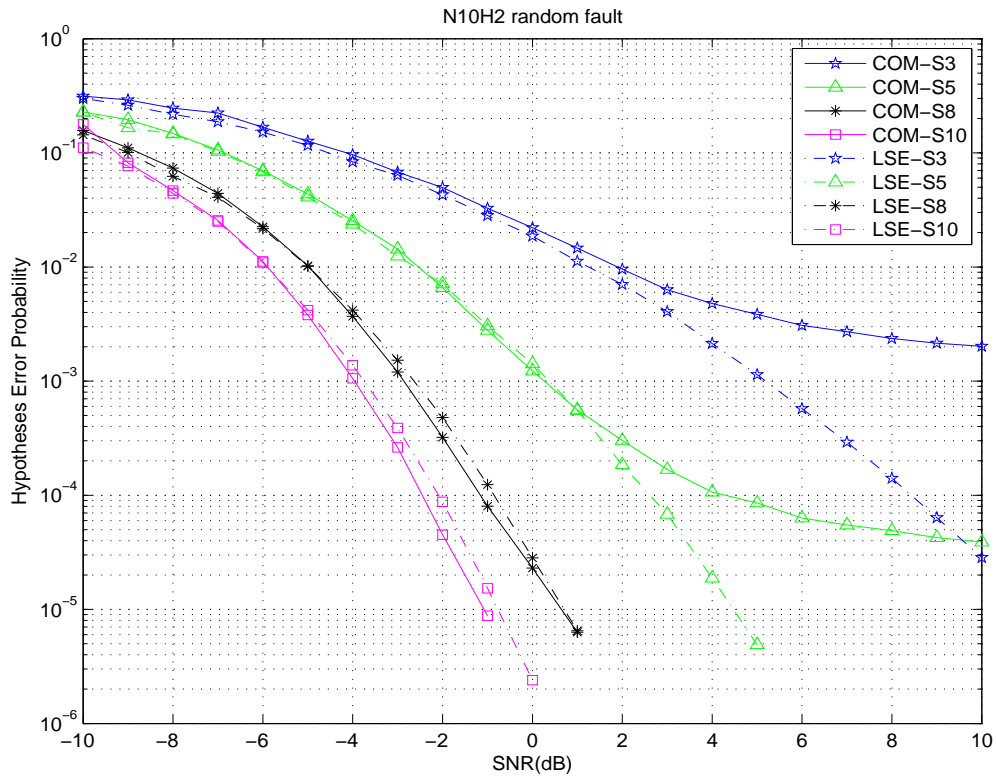


Figure 3.18: Performance of hypothesis detection. “N10H2 random fault” represents 10 bits per sensor, two hypotheses and one random faulty sensor are assumed in this figure.

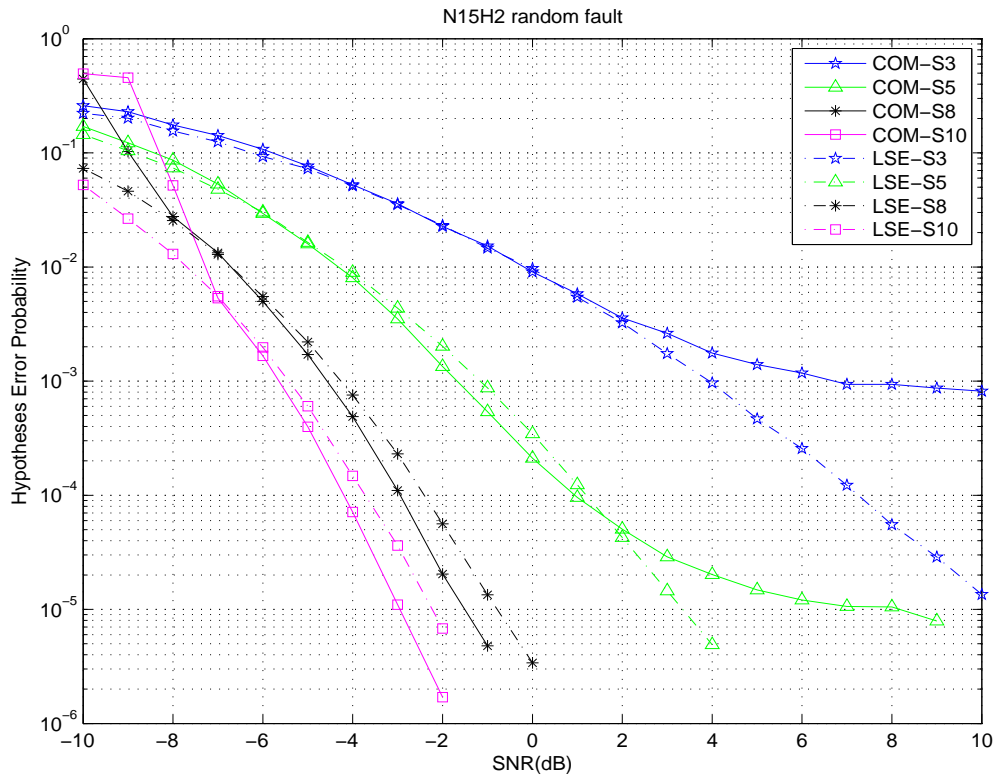


Figure 3.19: Performance of hypothesis detection. “N15H2 random fault” represents 15 bits per sensor, two hypotheses and one random faulty sensor are assumed in this figure.

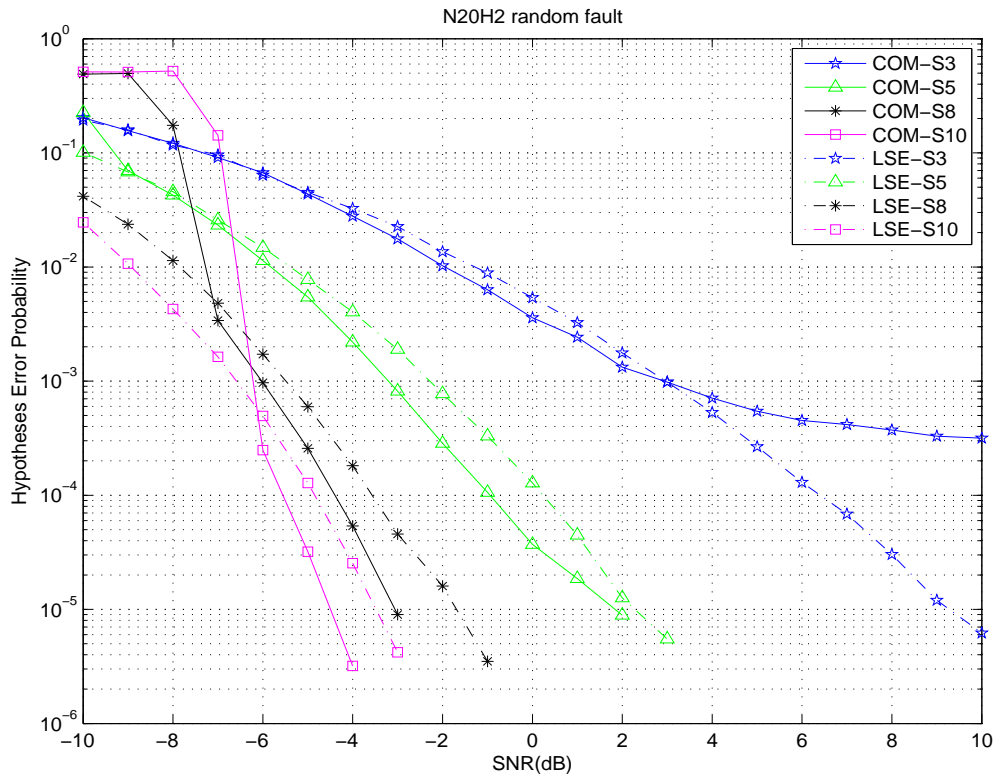


Figure 3.20: Performance of hypothesis detection. “N20H2 random fault” represents 20 bits per sensor, two hypotheses and one random faulty sensor are assumed in this figure.

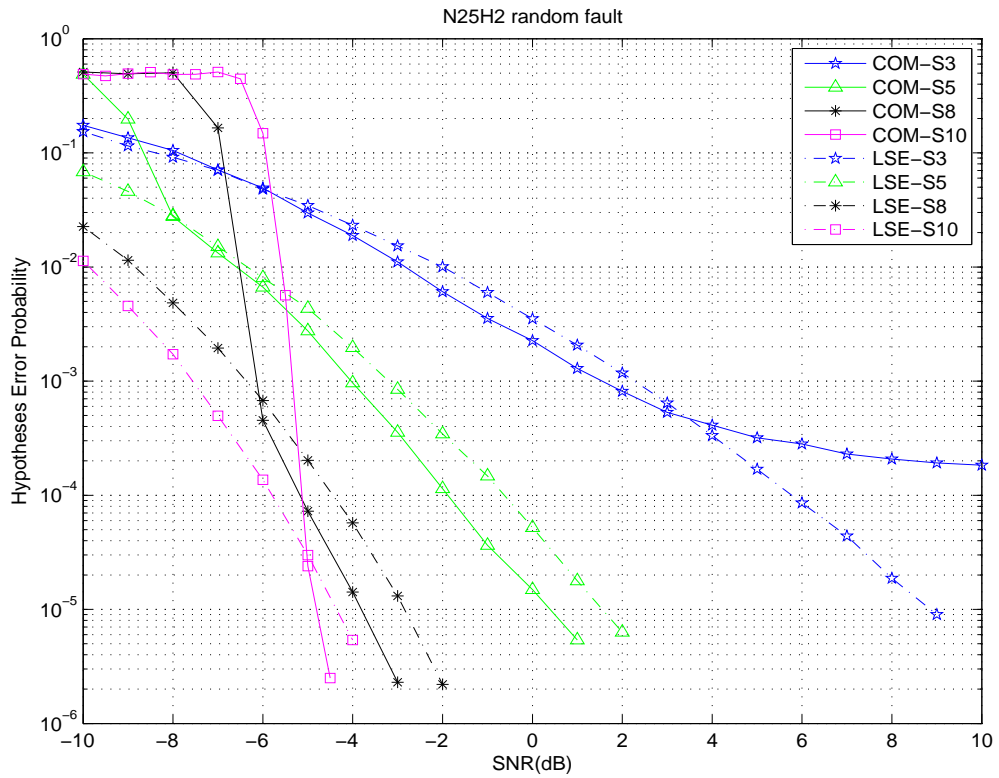


Figure 3.21: Performance of hypothesis detection. “N25H2 random fault” represents 25 bits per sensor, two hypotheses and one random faulty sensor are assumed in this figure.

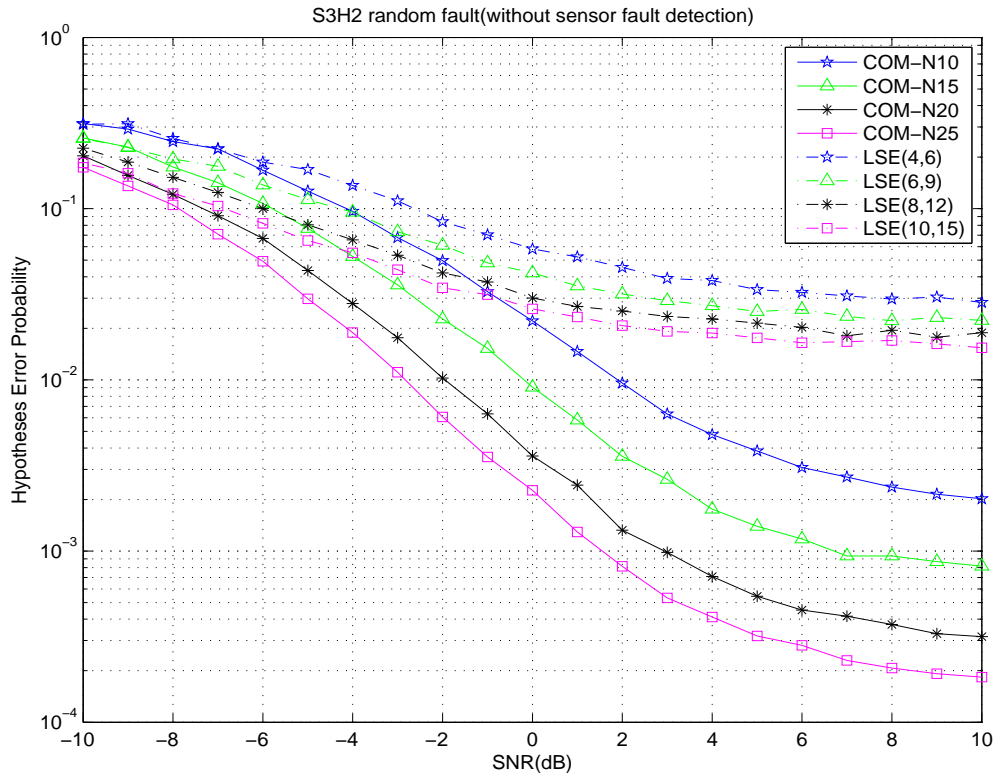


Figure 3.22: Performance of hypothesis detection. “S3H2 random fault (without sensor fault detection)” represents three sensors, two hypotheses, one random faulty sensor, and no faulty-sensor detection at the LSE fusion are assumed in this figure.

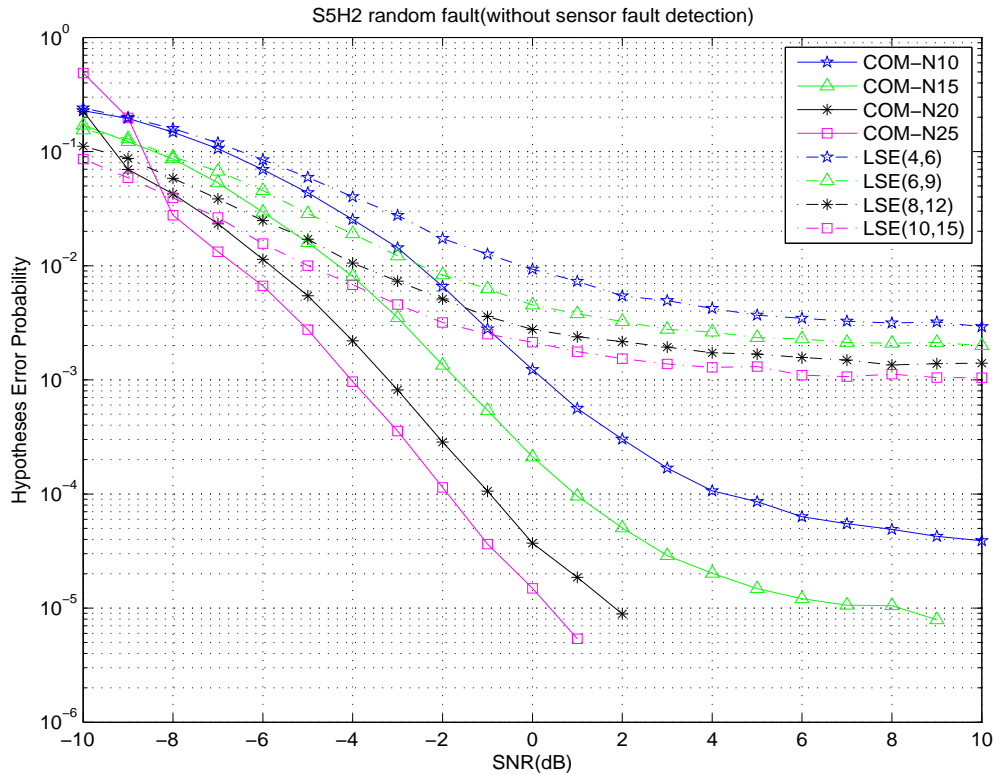


Figure 3.23: Performance of hypothesis detection. “S5H2 random fault(without sensor fault detection)” represents five sensors, two hypotheses, one random faulty sensor, and no faulty-sensor detection at the LSE fusion are assumed in this figure.

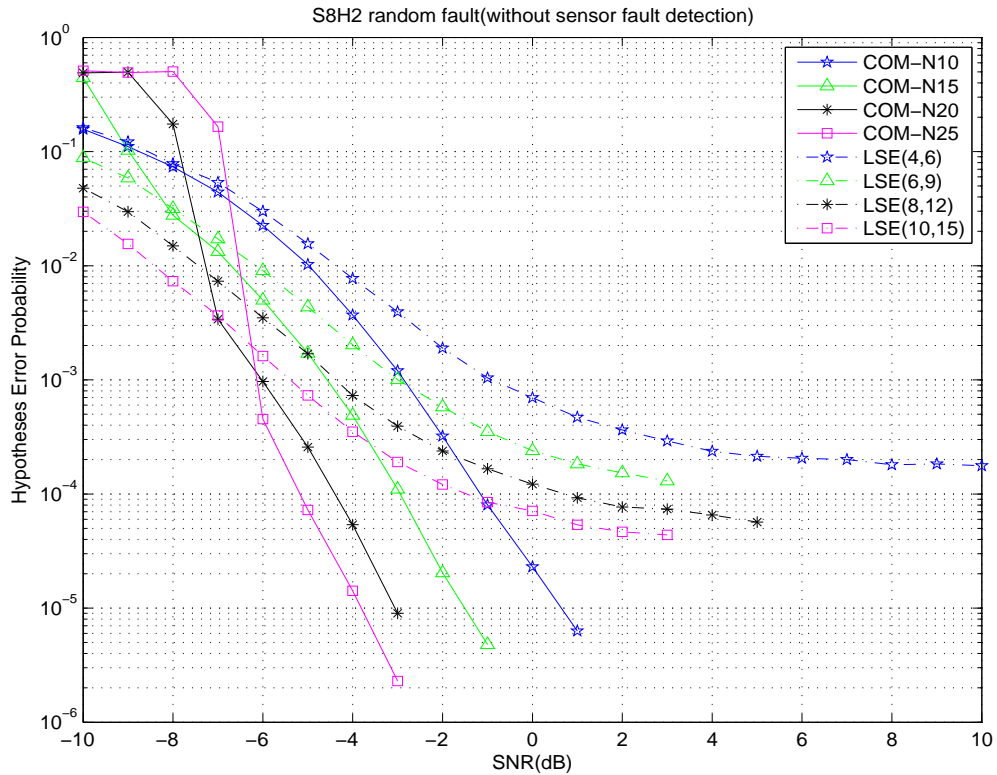


Figure 3.24: Performance of hypothesis detection. “S8H2 random fault (without sensor fault detection)” represents eight sensors, two hypotheses, one random faulty sensor, and no faulty-sensor detection at the LSE fusion are assumed in this figure.

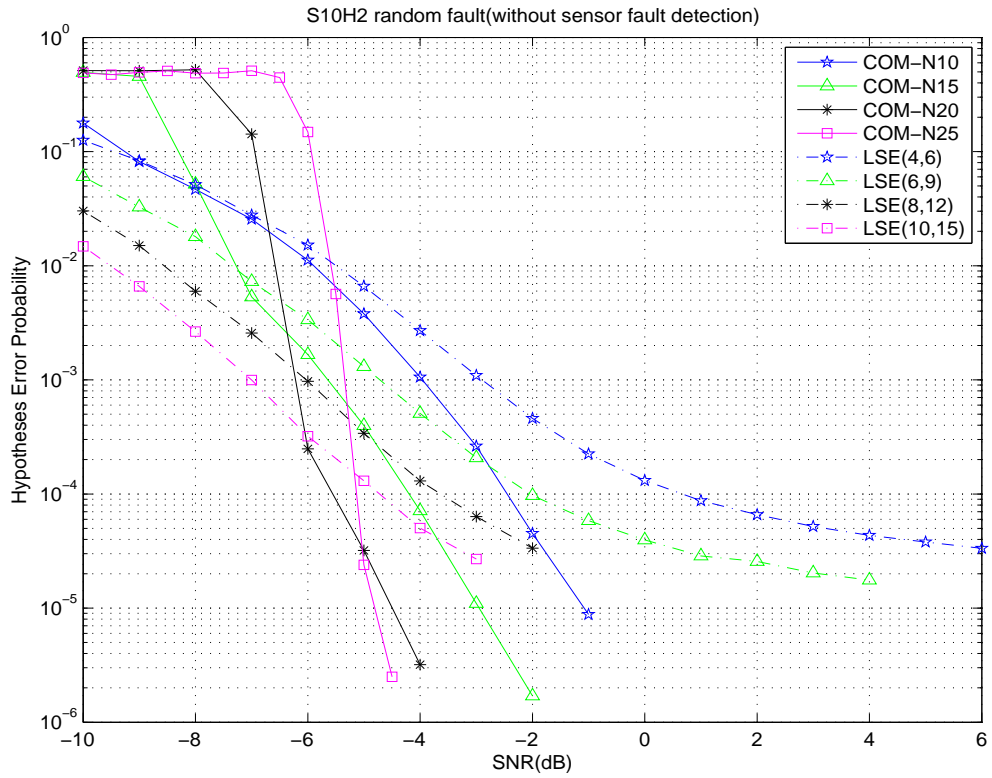


Figure 3.25: Performance of hypothesis detection. “S10H2 random fault(without sensor fault detection)” represents ten sensors, two hypotheses, one random faulty sensor, and no faulty-sensor detection at the LSE fusion are assumed in this figure.

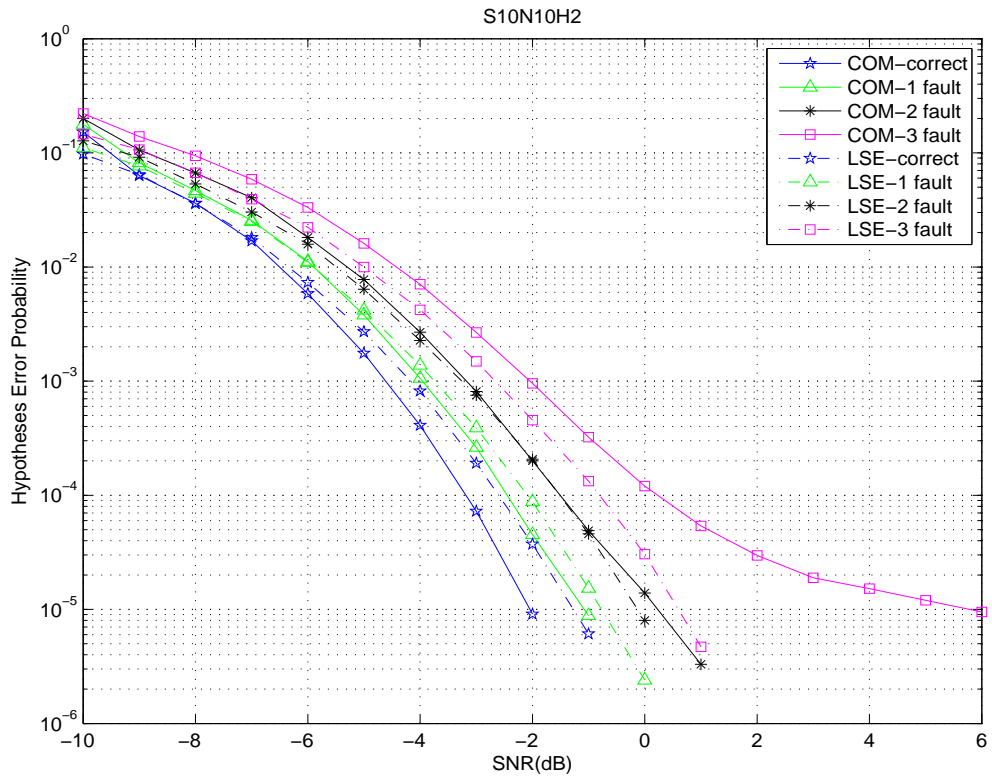


Figure 3.26: Performance of hypothesis detection. “S10N10H2” represents ten sensors, 10 bits per sensor and two hypotheses are assumed in this figure.

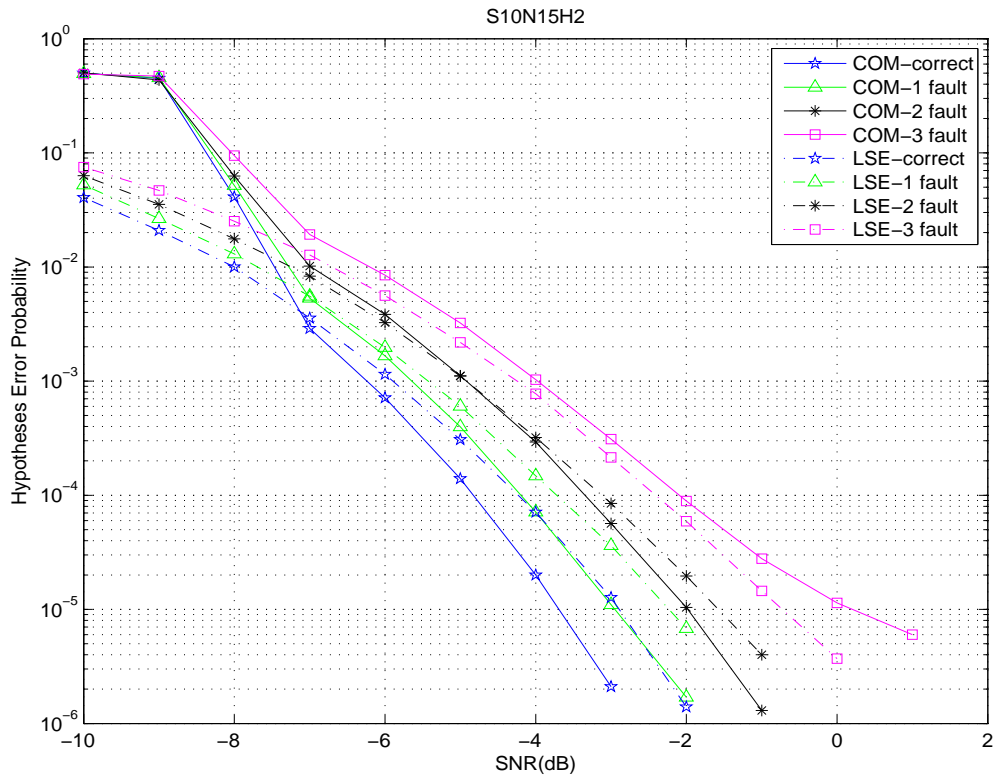


Figure 3.27: Performance of hypothesis detection. “S10N15H2” represents ten sensors, 15 bits per sensor and two hypotheses are assumed in this figure.

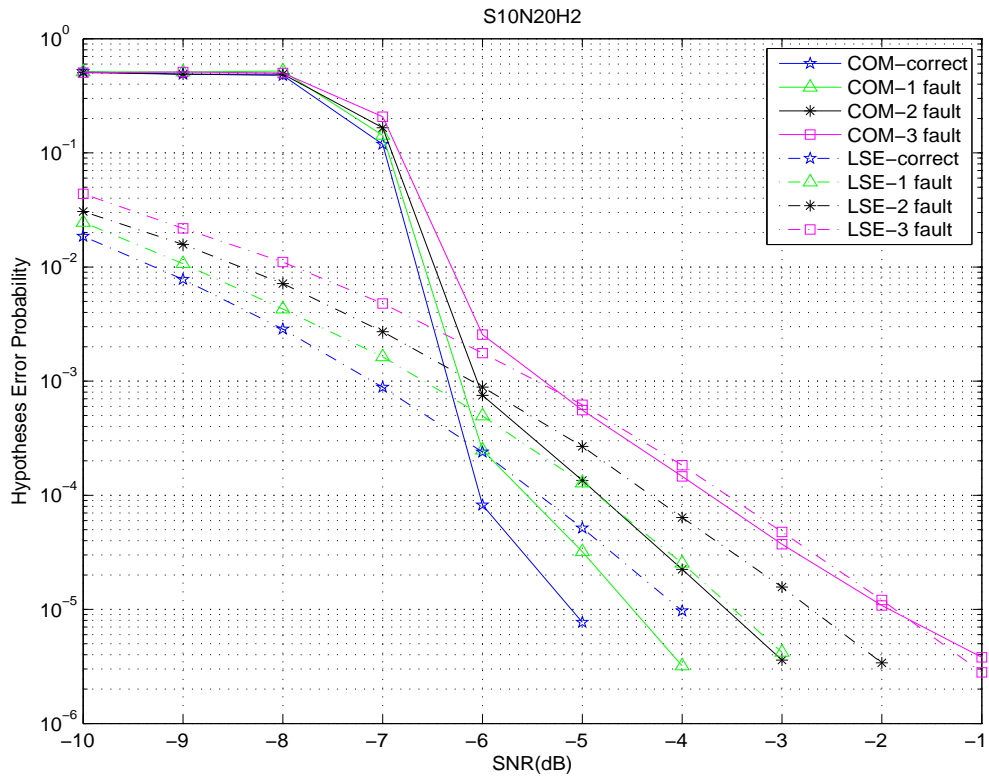


Figure 3.28: Performance of hypothesis detection. “S10N20H2” represents ten sensors, 20 bits per sensor and two hypotheses are assumed in this figure.

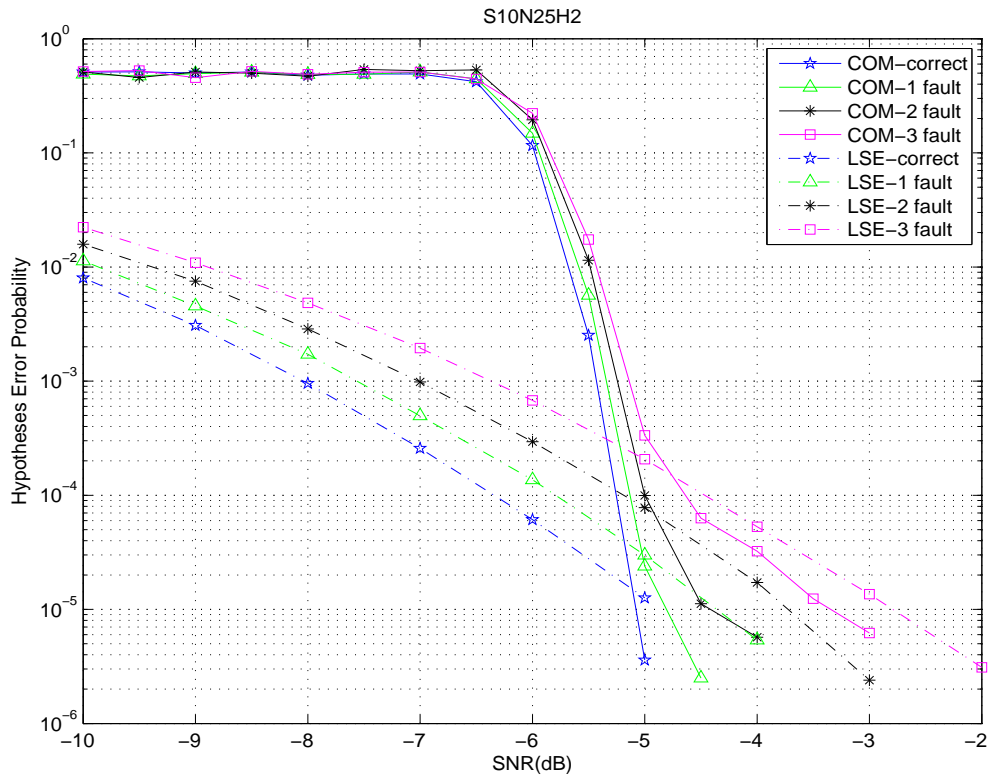


Figure 3.29: Performance of hypothesis detection. “S10N25H2” represents ten sensors, 25 bits per sensor and two hypotheses are assumed in this figure.

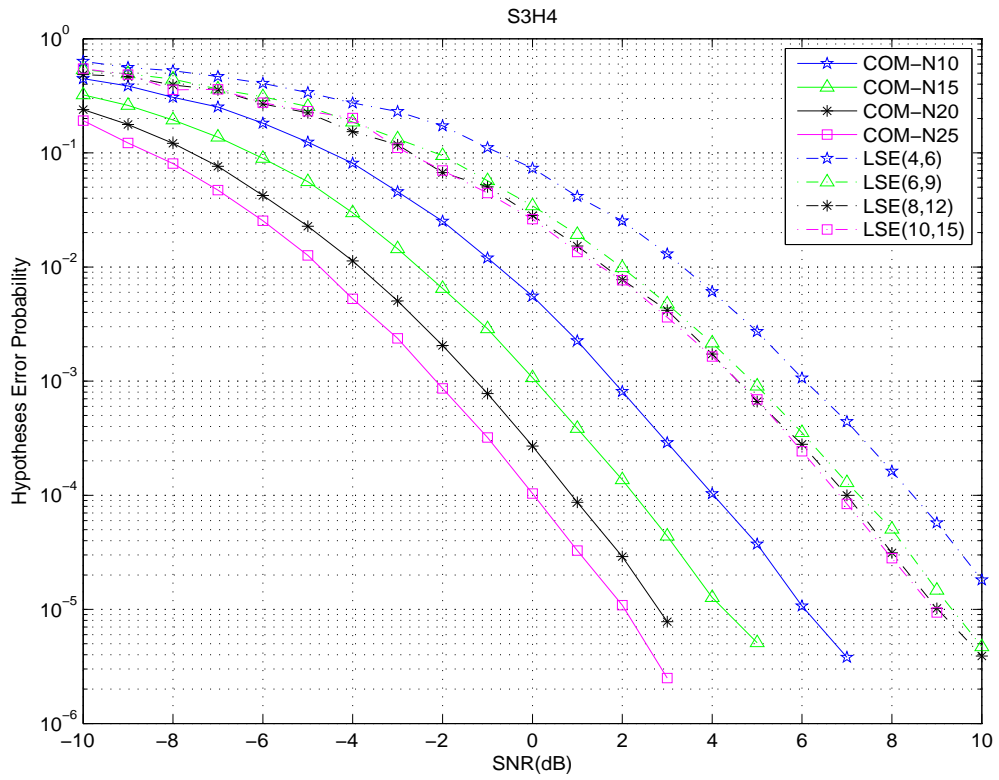


Figure 3.30: Performances of hypothesis detection. “S3H4” represents three sensors and four hypotheses are assumed in this figure.

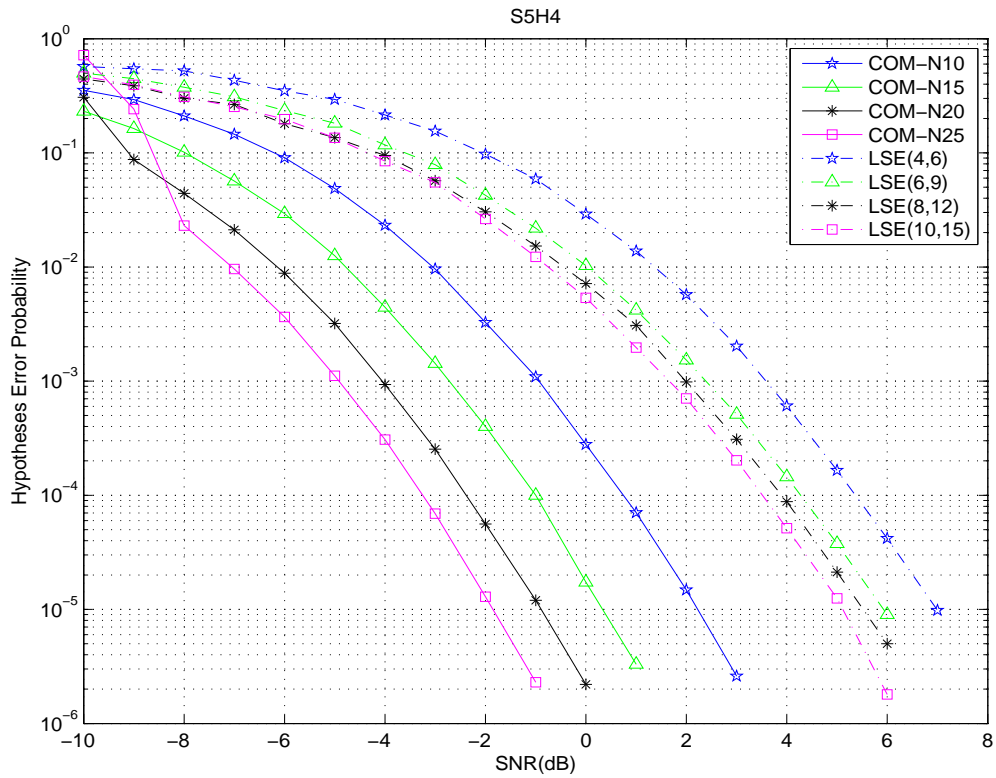


Figure 3.31: Performances of hypothesis detection. “S5H4” represents five sensors and four hypotheses are assumed in this figure.

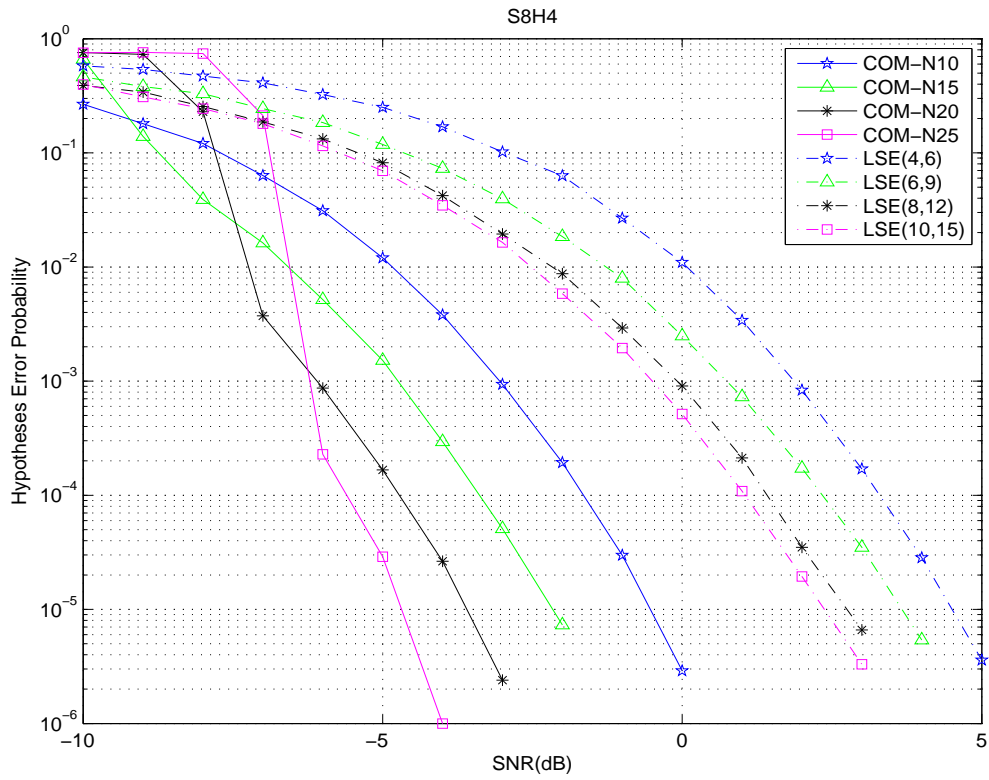


Figure 3.32: Performances of hypothesis detection. “S8H4” represents eight sensors and four hypotheses are assumed in this figure.

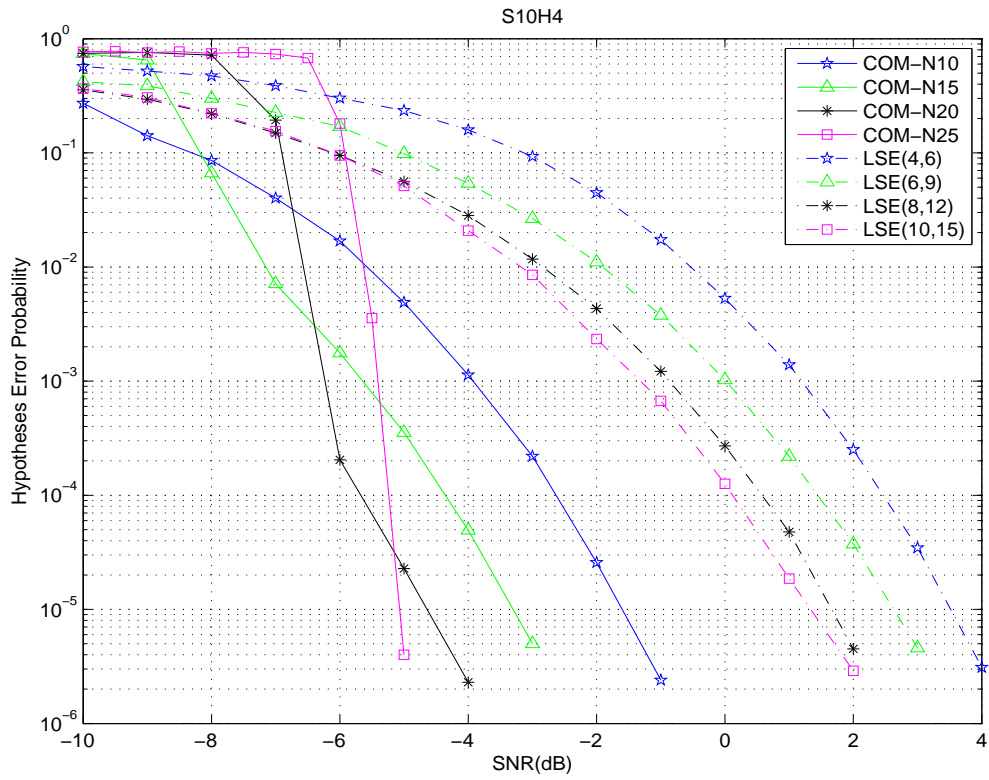


Figure 3.33: Performances of hypothesis detection. “S10H4” represents ten sensors and four hypotheses are assumed in this figure.

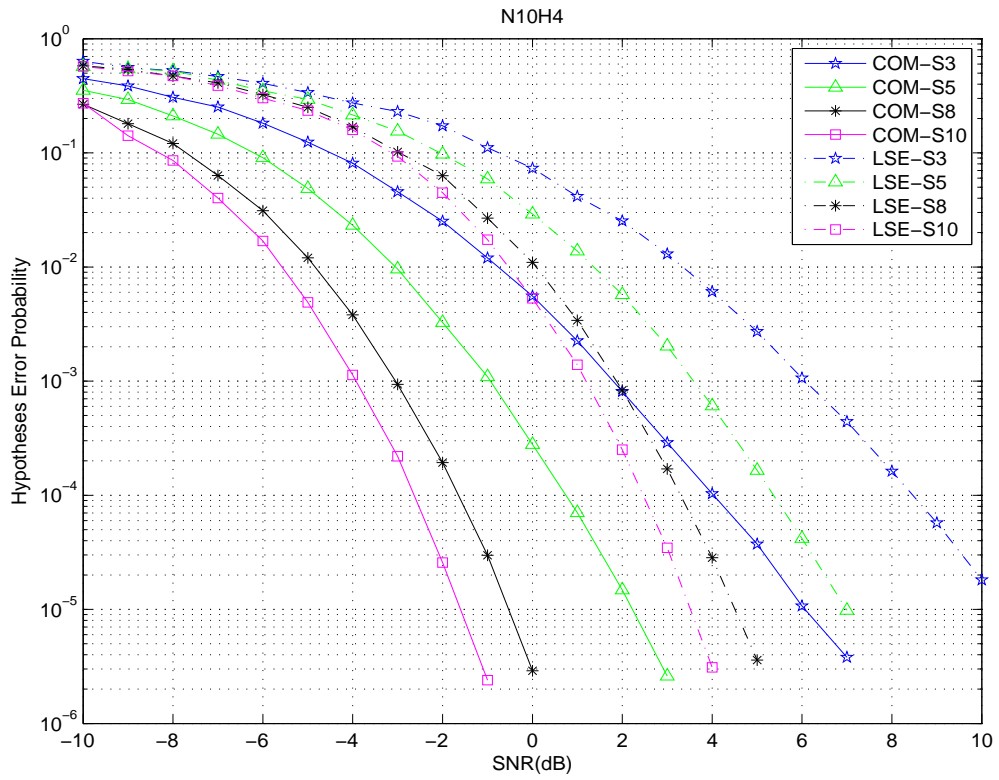


Figure 3.34: Performances of hypothesis detection. “N10H4” represents 10 bits per sensor and four hypotheses are assumed in this figure.

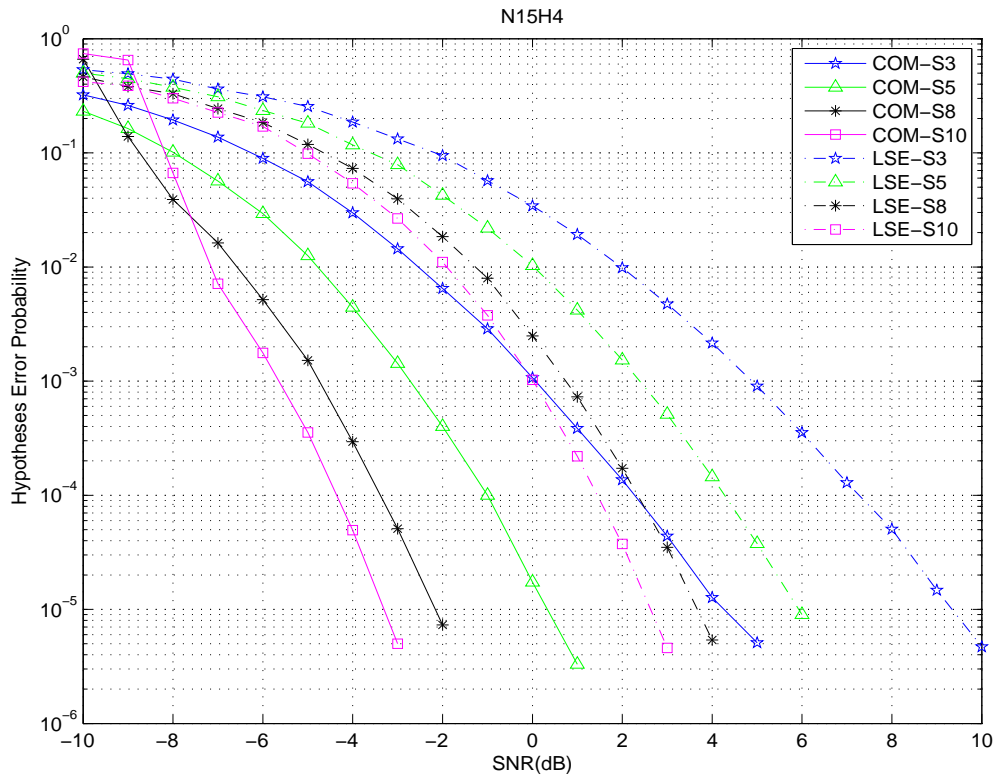


Figure 3.35: Performances of hypothesis detection. “N15H4” represents 15 bits per sensor and four hypotheses are assumed in this figure.

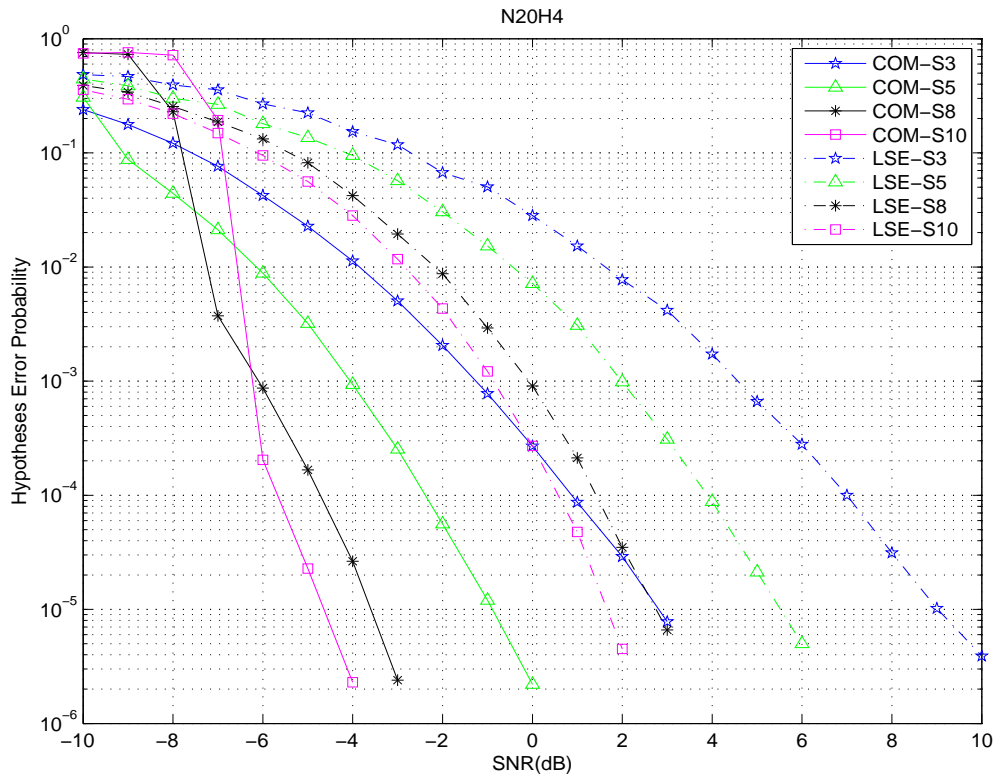


Figure 3.36: Performances of hypothesis detection. “N20H4” represents 20 bits per sensor and four hypotheses are assumed in this figure.

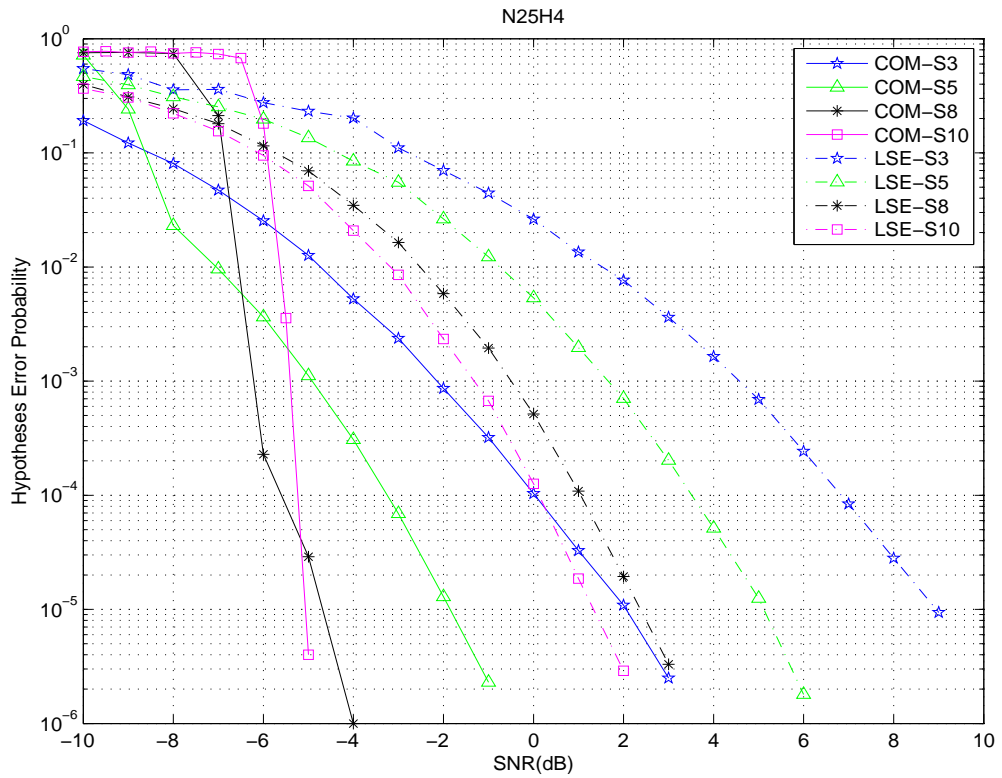


Figure 3.37: Performances of hypothesis detection. “N25H4” represents 25 bits per sensor and four hypotheses are assumed in this figure.

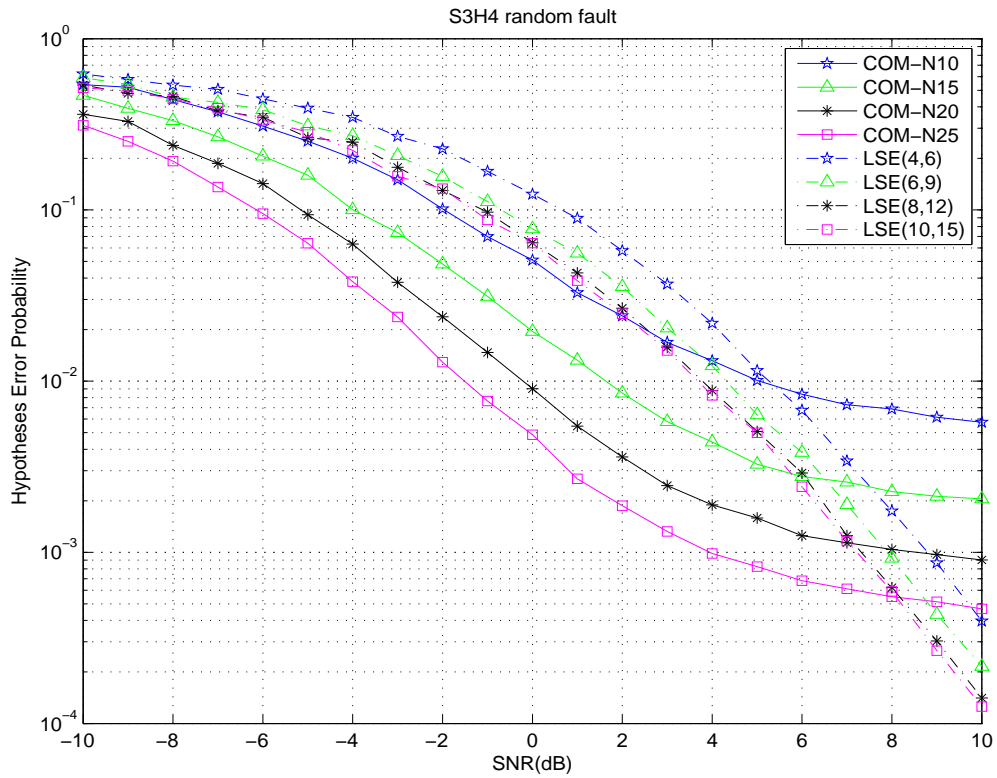


Figure 3.38: Performance of hypothesis detection. “S3H4 random fault” represents three sensors, four hypotheses and one random faulty sensor are assumed in this figure.

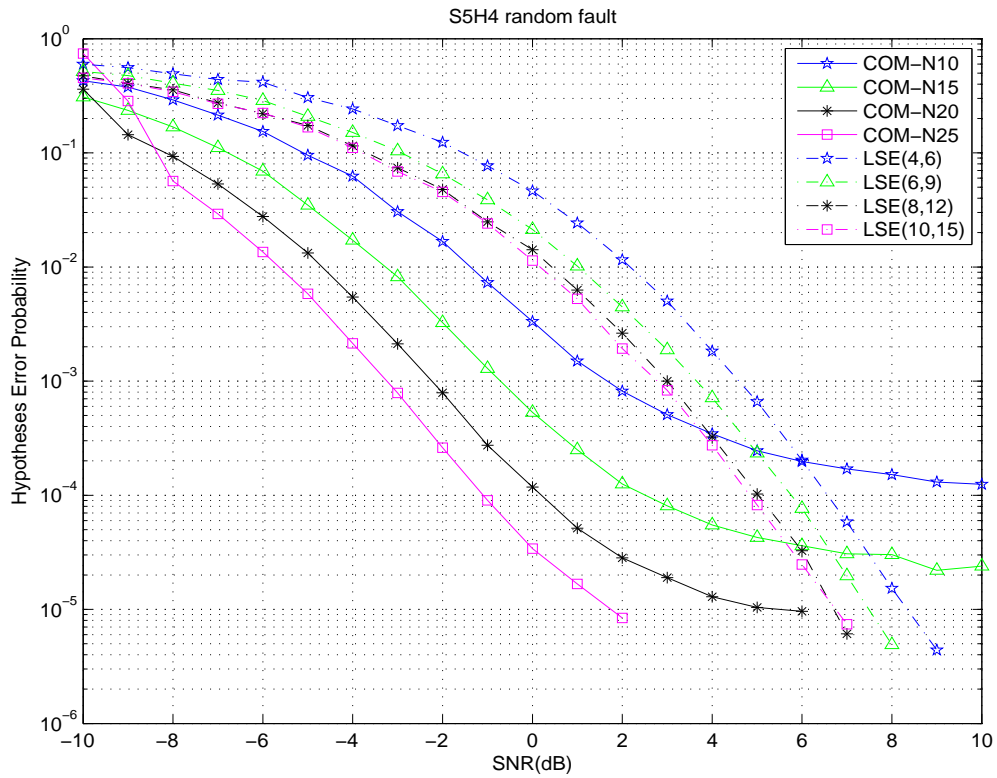


Figure 3.39: Performance of hypothesis detection. “S5H4 random fault” represents five sensors, four hypotheses and one random faulty sensor are assumed in this figure.

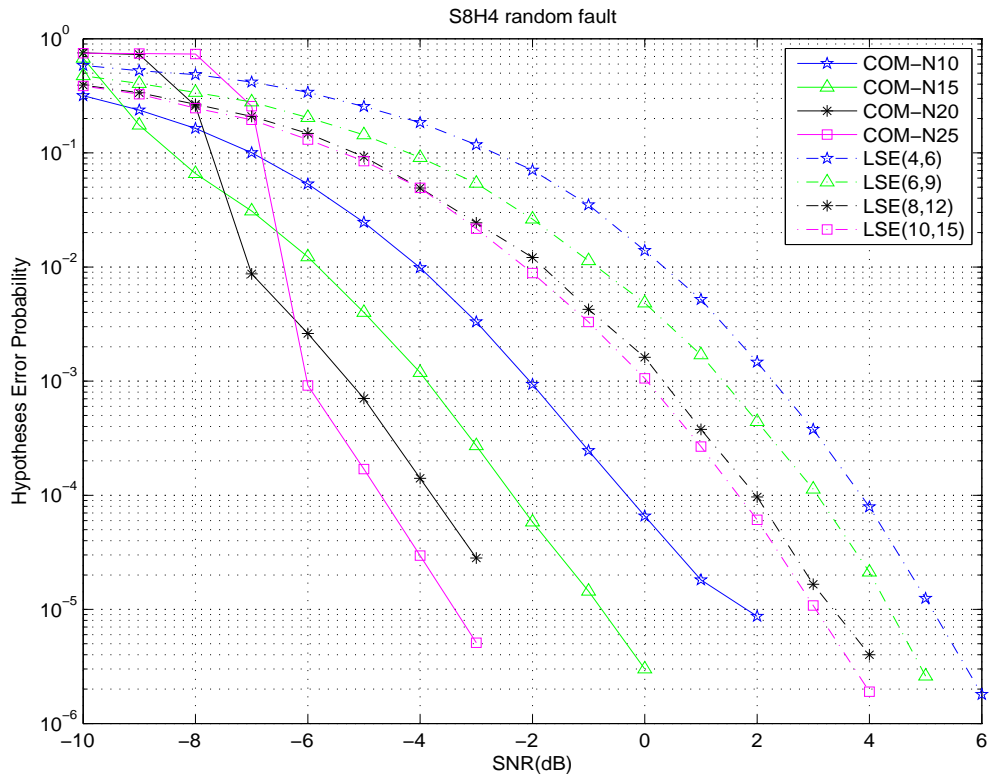


Figure 3.40: Performance of hypothesis detection. “S8H4 random fault” represents eight sensors, four hypotheses and one random faulty sensor are assumed in this figure.

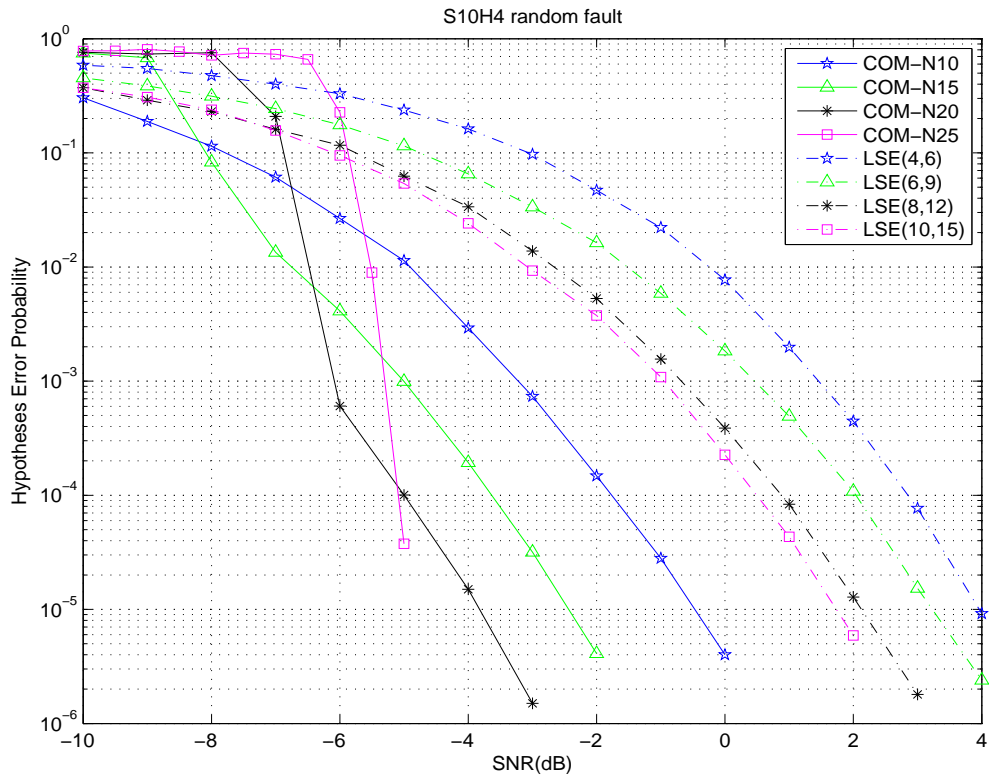


Figure 3.41: Performance of hypothesis detection. “S10H4 random fault” represents ten sensors, four hypotheses and one random faulty sensor are assumed in this figure.

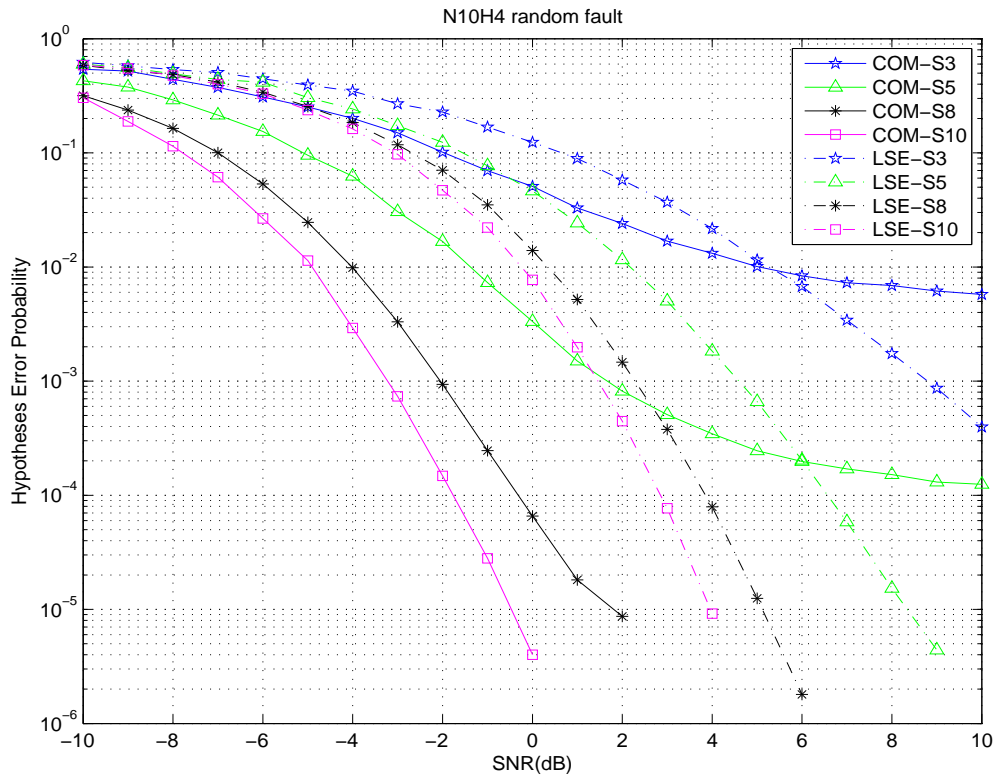


Figure 3.42: Performance of hypothesis detection. “N10H4 random fault” represents 10 bits per sensor, four hypotheses and one random faulty sensor are assumed in this figure.

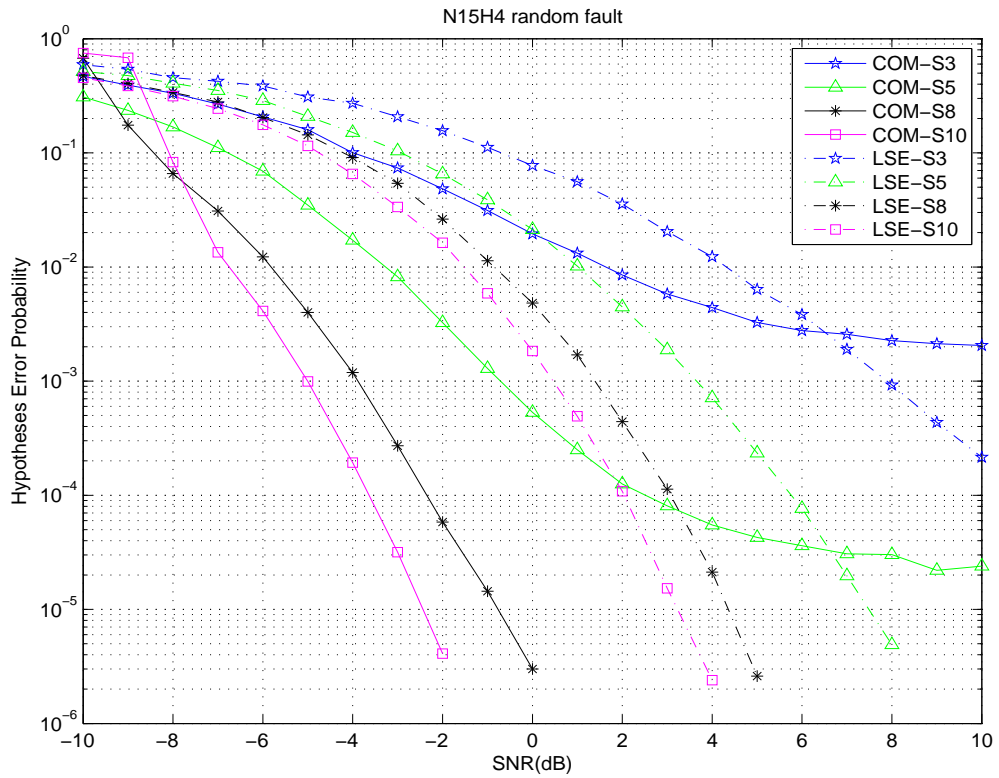


Figure 3.43: Performance of hypothesis detection. “N15H4 random fault” represents 15 bits per sensor, four hypotheses and one random faulty sensor are assumed in this figure.

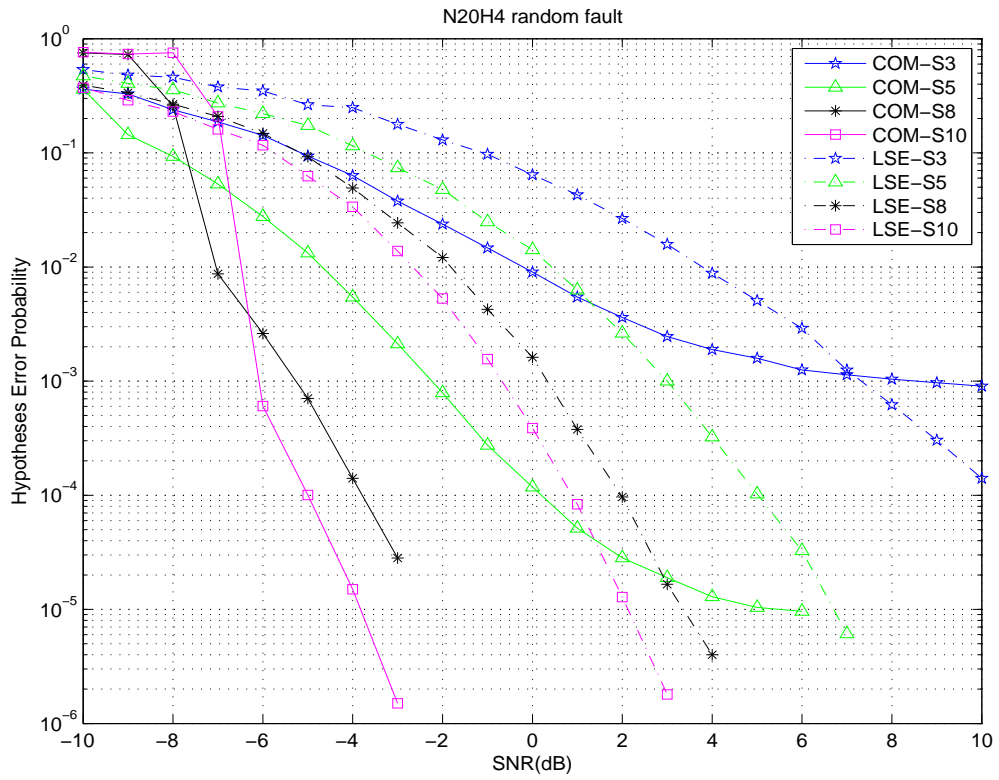


Figure 3.44: Performance of hypothesis detection. “N20H4 random fault” represents 20 bits per sensor, four hypotheses and one random faulty sensor are assumed in this figure.

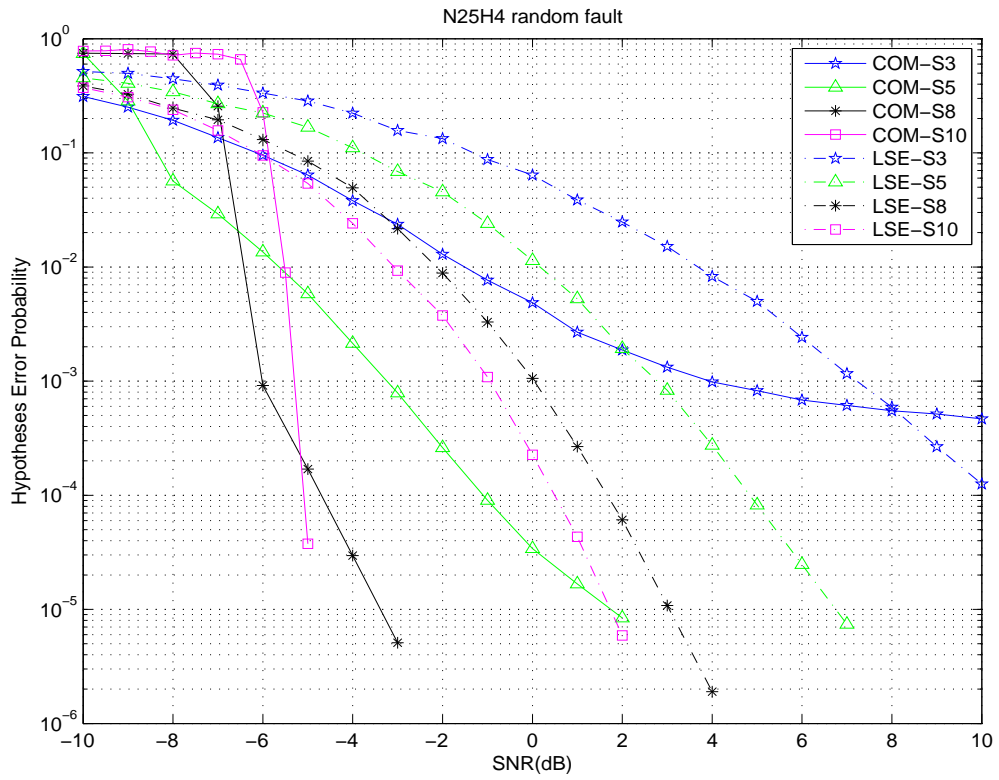


Figure 3.45: Performance of hypothesis detection. “N25H4 random fault” represents 25 bits per sensor, four hypotheses and one random faulty sensor are assumed in this figure.

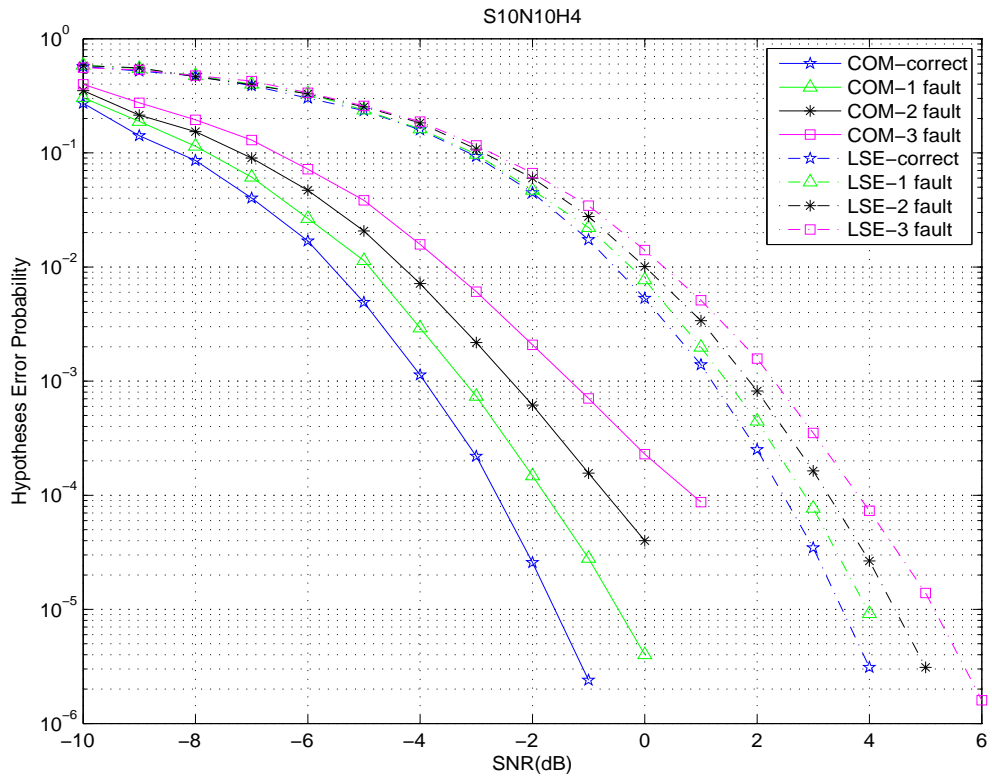


Figure 3.46: Performance of hypothesis detection. “S10N10H4” represents ten sensors, 10 bits per sensor and four hypotheses are assumed in this figure.

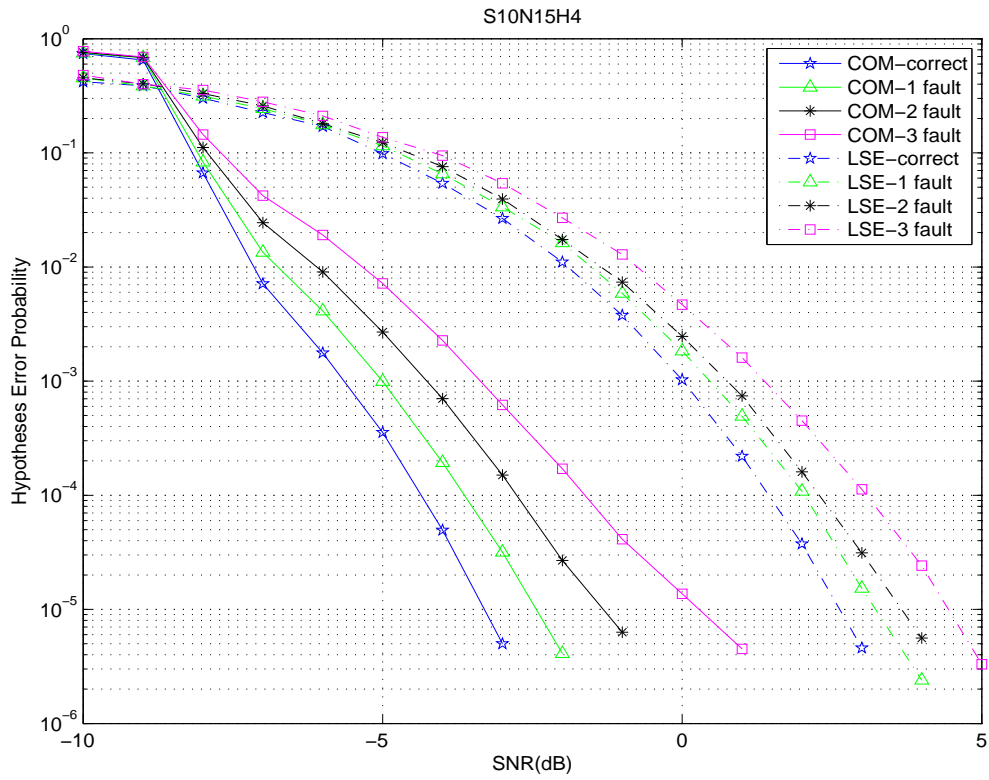


Figure 3.47: Performance of hypothesis detection. “S10N15H4” represents ten sensors, 15 bits per sensor and four hypotheses are assumed in this figure.

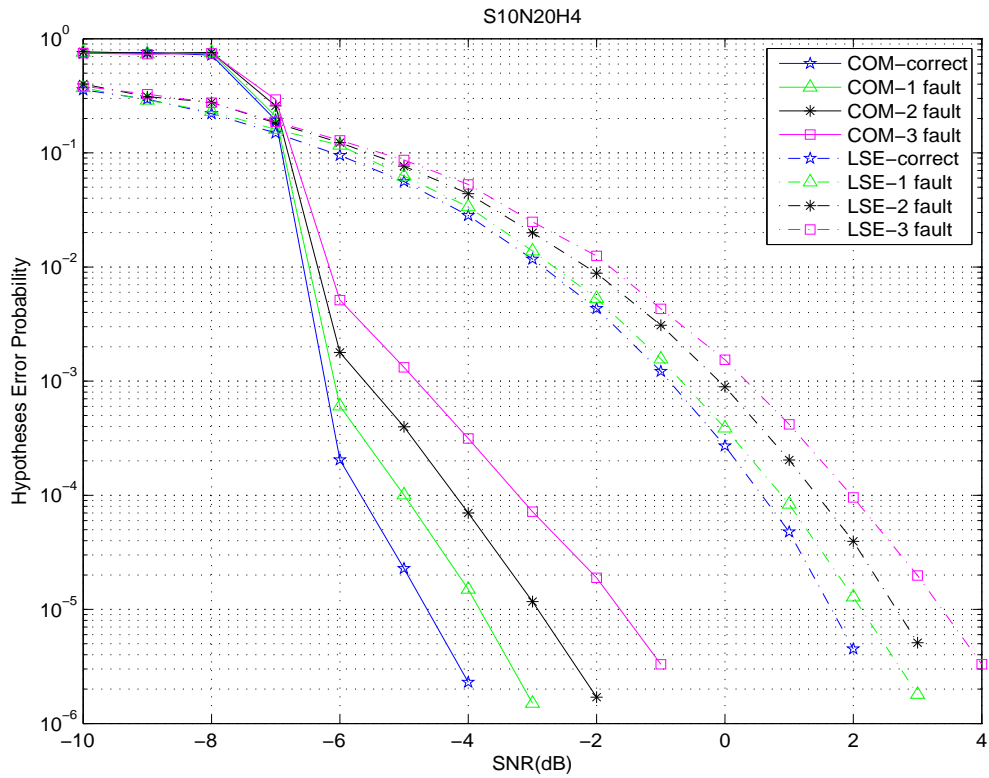


Figure 3.48: Performance of hypothesis detection. “S10N20H4” represents ten sensors, 20 bits per sensor and four hypotheses are assumed in this figure.

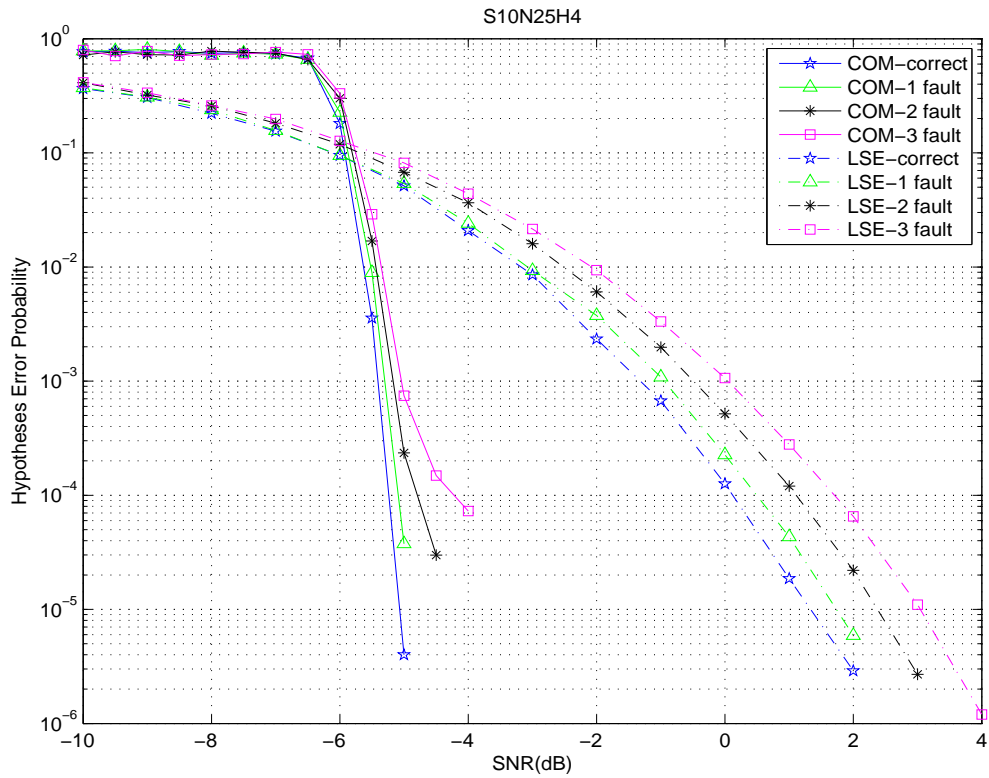


Figure 3.49: Performance of hypothesis detection. “S10N25H4” represents ten sensors, 25 bits per sensor and four hypotheses are assumed in this figure.

Chapter 4

Amendment to Deep Fading by Quantization

In chapter 3, we observe the sudden performance degradation due to deep fading at low SNR in our COM scheme when $S \times N$ is more than 100. This observation cut short the value of the COM scheme at low SNR when it is compared with the conventional LSE scheme. In principle, the deep fading effect will make the channel coefficients become transiently small, and hence, contribute a large untrustworthy soft branch metric value to the entire metric sum on which the soft fusion decision is based. By employing hard-decision fusion, the influence of such transient fades to the overall metric sum can be limited, and the sudden performance degradation is anticipated to be alleviated. Simulations in Figs. 3.10-3.13 have already confirmed our anticipation. However, the hard-decision fusion, although eliminating the deep-fade sudden performance degradation, unfortunately performs a little worse than the LSE scheme.

In this chapter, we attempt to perform a finer quantization (than the hard-decision one) at the fusion center such that better performance for the COM scheme (than the soft-decision LSE scheme) can be obtained without the deep fading performance degradation.

Table 4.1: The optimum uniform step size for gaussian random variable

Number of quantization bits	1	2	3	4	5
Number of output levels	2	4	8	16	32
Optimum step size	1.596	0.9957	0.586	0.3352	0.1881

4.1 Quantization of The Reception

According to the channel model in Chapter 2, the received vector \mathbf{r} is complex Gaussian distributed. We can then adopt the method in [6] to find the optimum uniform step size that minimizes the mean square quantization error as listed in Table 4.1.

Figure 4.1 shows that both 2-bit and 3-bit quantization can help preventing the sudden performance degradation due to deep fading. Even at high SNRs, the 3-bit quantization at the fusion center is only 0.2 dB inferior to the soft-decision fusion.

Figures 4.2 and 4.3 compare the performances of 3-bit quantized COM fusion and LSE fusion with/without sensor fault. As anticipated, the 3-bit quantized COM scheme performs better than the LSE scheme at medium to high SNR; however, even almost eliminating the deep fading effect, it still performs a little worse than the LSE scheme at low SNR.

For a fair comparison, we also provide figures in which both COM and LSE fusion decisions are based on 3-bit quantized reception. Figures 4.4 and 4.5 compare the performances of 3-bit quantized COM fusion and 3-bit quantized LSE fusion with/without sensor fault. In such case, the performance of the 3-bit quantized COM scheme is apparently better than the 3-bit quantized LSE scheme except for the SNR range where sudden performance drop due to deep fading occurs.

Notably, in the above four figures, when $S \times N$ exceeds 250, the sudden performance degradation still occurs at low SNR. As the decision criterion in (2.2) can be equivalently

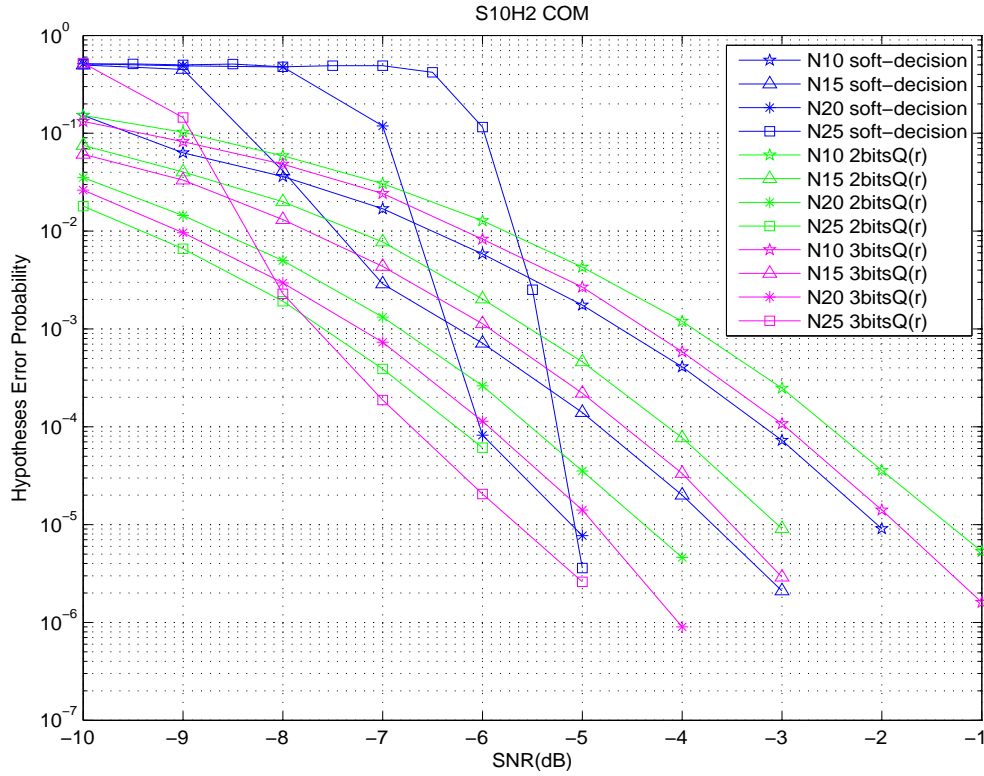


Figure 4.1: Performance of quantized and soft-decision COM fusions. “S10H2” represents ten sensors and two hypotheses are assumed in this figure. “3bitsQ(r)” means 3-bit quantizer is used in the quantization of reception \mathbf{r} .

transformed to

$$\hat{\ell} = \arg \min_{1 \leq \ell \leq M} \sum_{k=1}^K \left\| \mathbf{r}_k \mathbf{r}_k^H - \mathbb{P}_{B_k}^{(\ell)} \right\|^2,$$

and the contribution of transient untrustworthy metric to the criterion sum is actually through the product form of two receptions, it is likely that performing quantization on each product of the receptions would be more reasonable and direct, for which the idea will be examined in the next section.

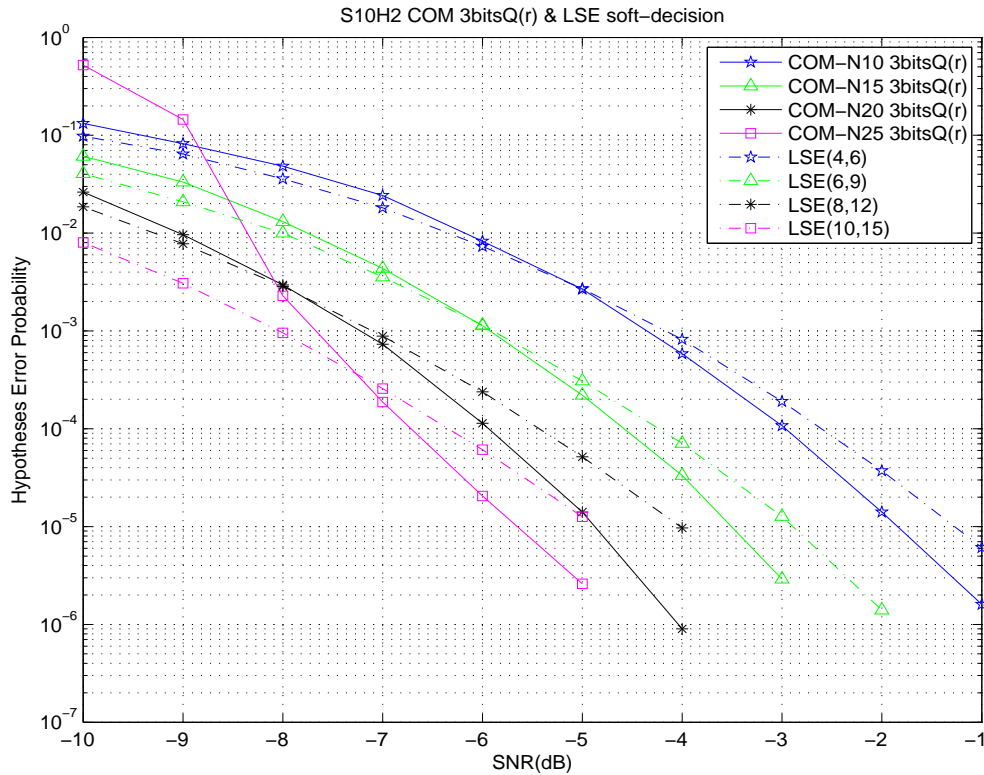


Figure 4.2: Performance of 3-bit quantized COM fusion and LSE fusion. “S10H2” represents ten sensors and two hypotheses are assumed in this figure. “3bitsQ(r)” means 3-bit quantizer is used in the quantization of reception r .

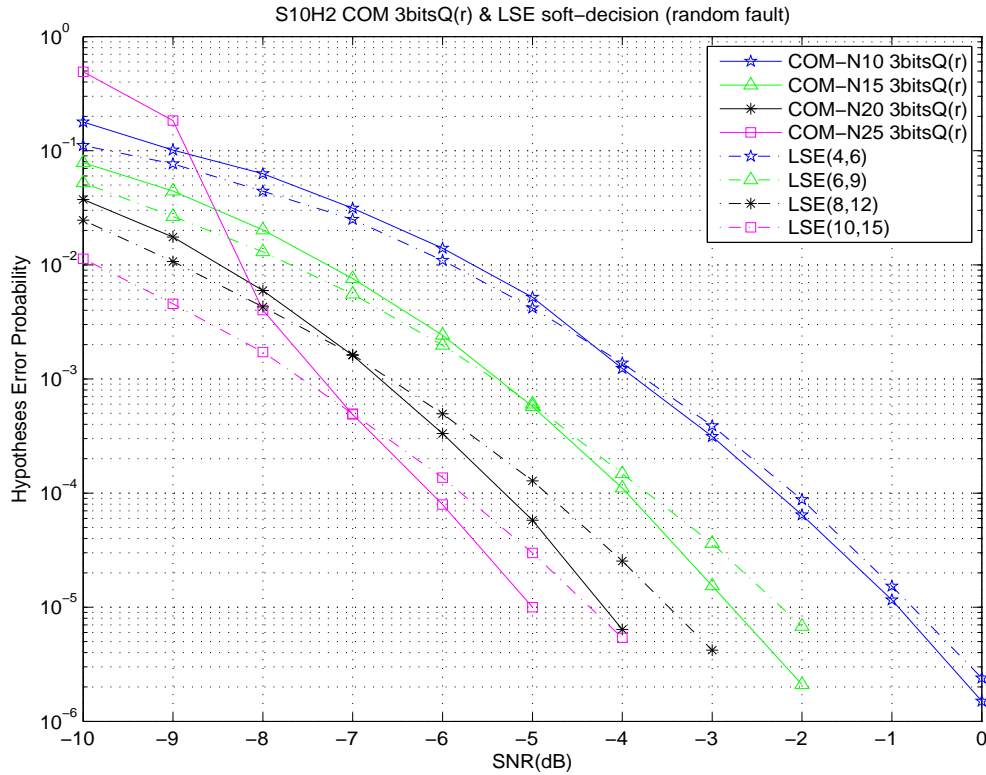


Figure 4.3: Performance of 3-bit quantized COM fusion and LSE fusion. “S10H2 . . . (random fault)” represents ten sensors, two hypotheses and one random faulty sensor are assumed in this figure. “3bitsQ(r)” means 3-bit quantizer is used in the quantization of reception \mathbf{r} .

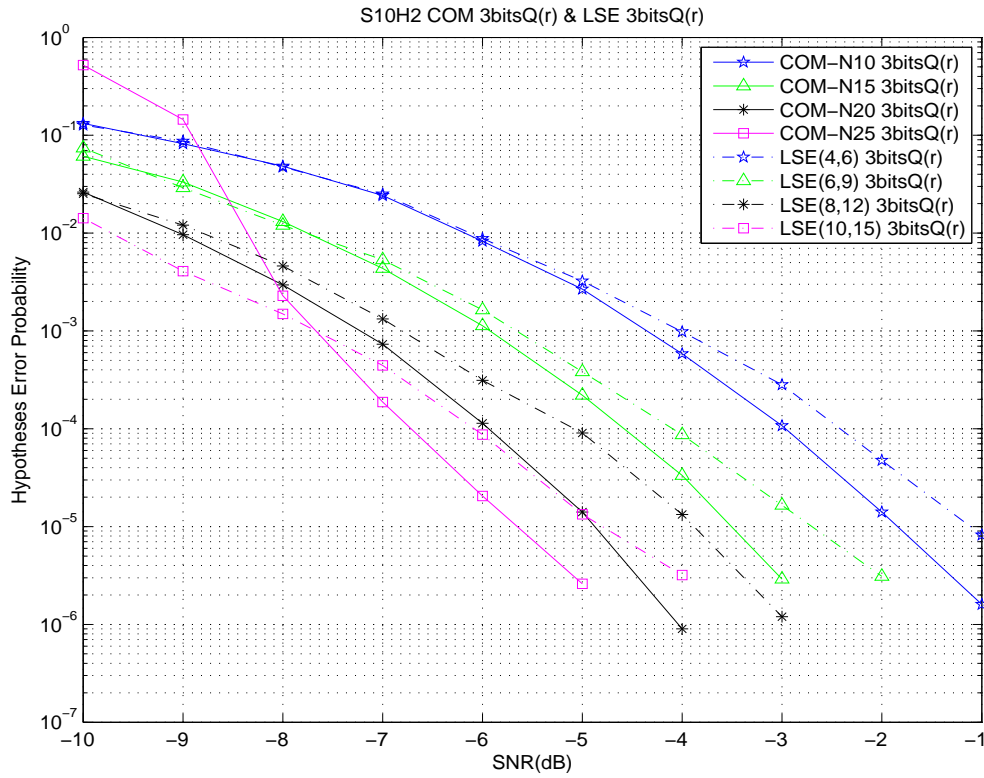


Figure 4.4: Performance of 3-bit quantized COM fusion and 3-bit quantized LSE fusion. “S10H2” represents ten sensors and two hypotheses are assumed in this figure. “3bitsQ(r)” means 3-bit quantizer is used in the quantization of reception r .

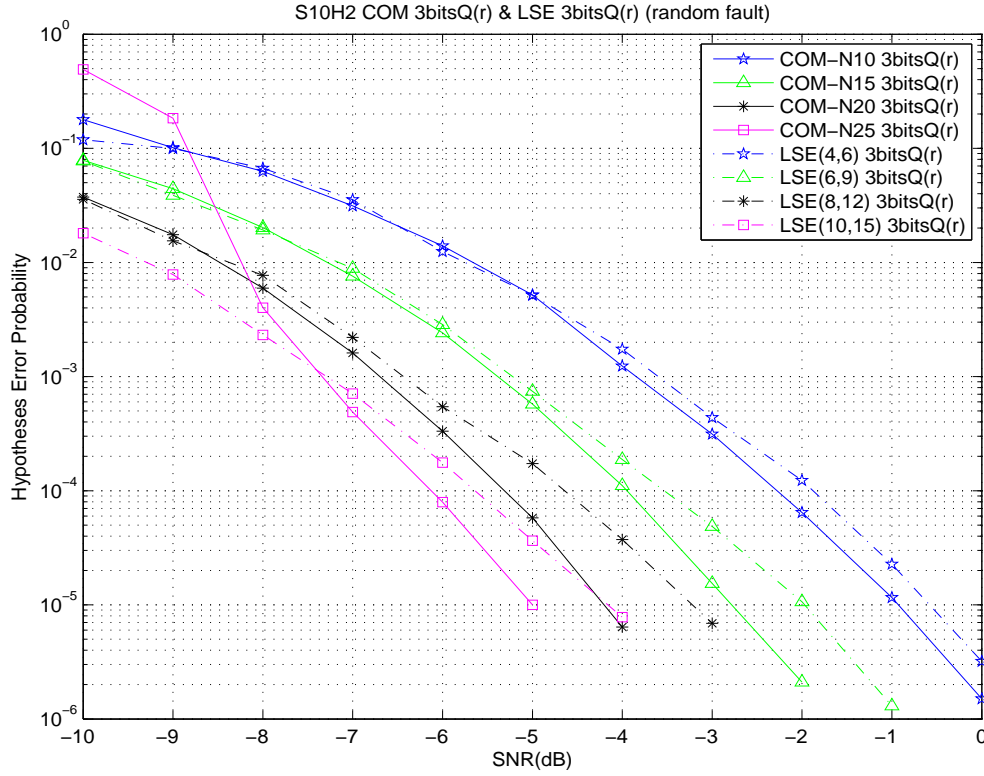


Figure 4.5: Performance of 3-bit quantized COM fusion and 3-bit quantized LSE fusion. “S10H2 \cdots (random fault)” represents ten sensors, two hypotheses and one random faulty sensor are assumed in this figure. “3bitsQ(r)” means 3-bit quantizer is used in the quantization of reception r .

4.2 Quantization of the Reception Product

In this section, we try to quantize the product value of $\mathbf{r}\mathbf{r}^H$, instead of \mathbf{r} itself. The same minimum-square-error method in Section 4.1 is used to find the uniform step size for reception product.

Figure 4.6 shows that the quantization on $\mathbf{r}\mathbf{r}^H$ can totally eliminate the sudden performance degradation due to deep fading.

Figures 4.7 and 4.8 again compare the performances of 3-bit product-quantized COM fusion and LSE fusion with/without sensor fault. The results indicate that the product-quantized COM scheme can compete with the LSE fusion in performance but without the effort of channel estimation and equalization.

For a fair comparison, we also provide figures in which the COM fusion decision is based on 3-bit product-quantized reception, and the LSE fusion decision is based on 3-bit quantized reception as shown in Figs. 4.9 and 4.10. Note that since the decision criterion of the LSE fusion is the Euclidean distance between the codeword and the received word, it is unnecessary to use product-quantization for the LSE fusion. The results indicate that the product-quantized COM scheme is a better choice than the quantized LSE scheme in performance.

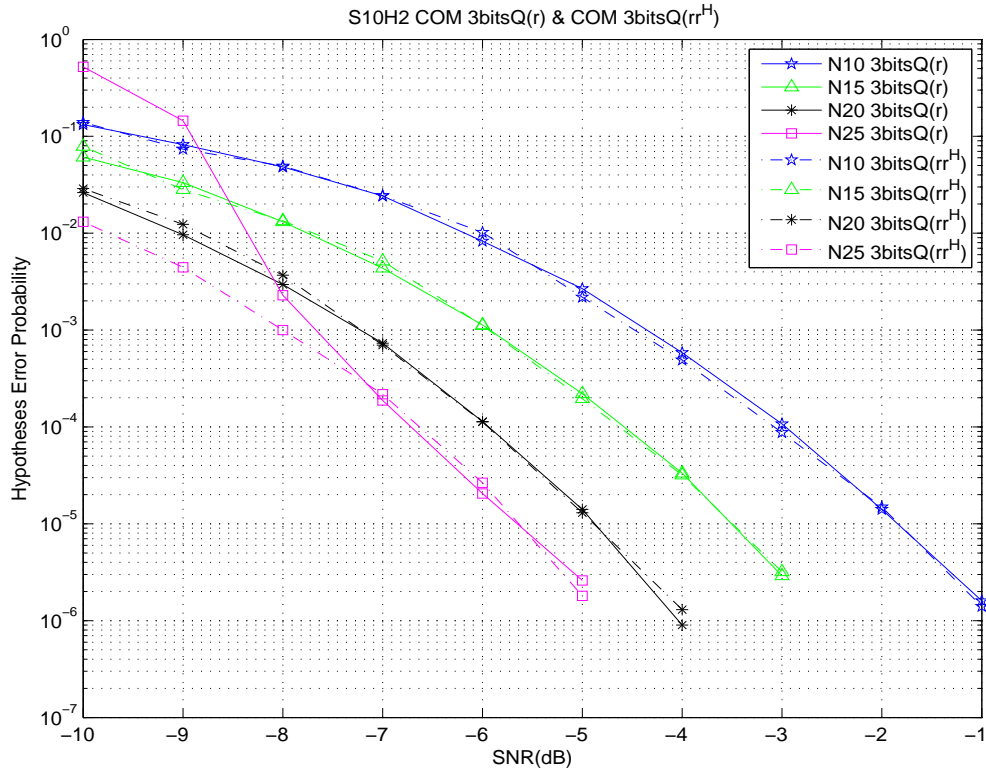


Figure 4.6: Performance of reception-quantized and reception-product quantized COM fusions. “S10H2” represents ten sensors and two hypotheses are assumed in this figure. “3bitsQ(r)” 3-bit quantizer is used in the quantization of reception r , while “3bitsQ(rr^H)” means 3-bit quantizer is used in the quantization of product reception rr^H .

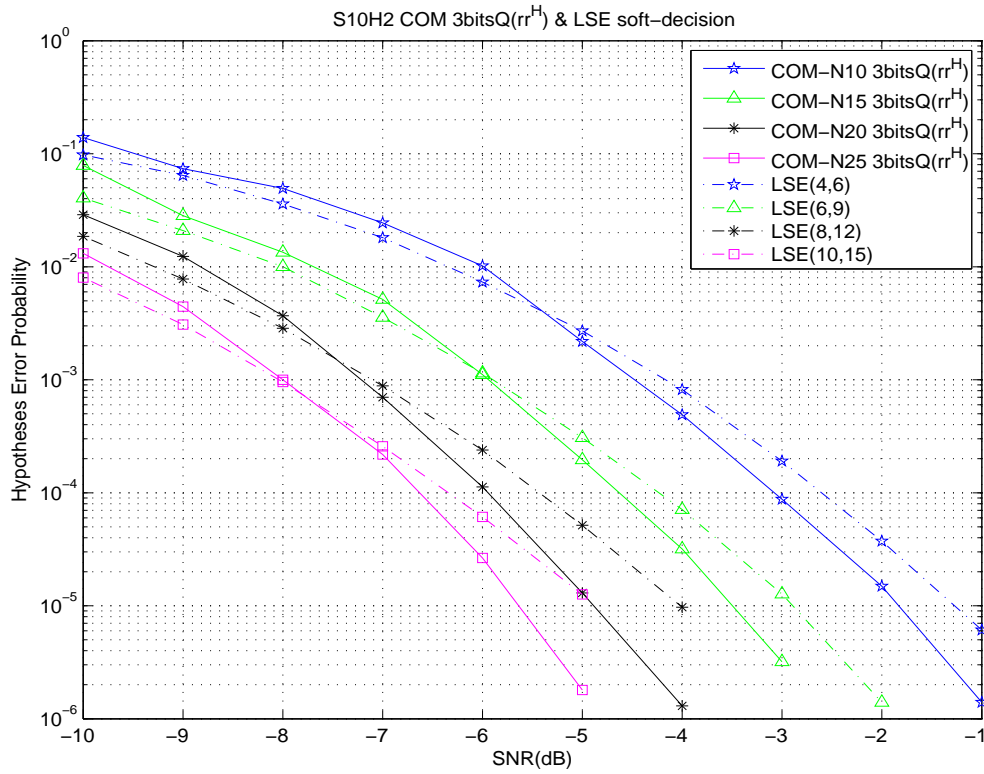


Figure 4.7: Performance of 3-bit reception-product-quantized COM fusion and LSE fusion. “S10H2” represents ten sensors and two hypotheses are assumed in this figure. “3bitsQ(rr^H)” means 3-bit quantizer is used in the quantization of product reception rr^H .

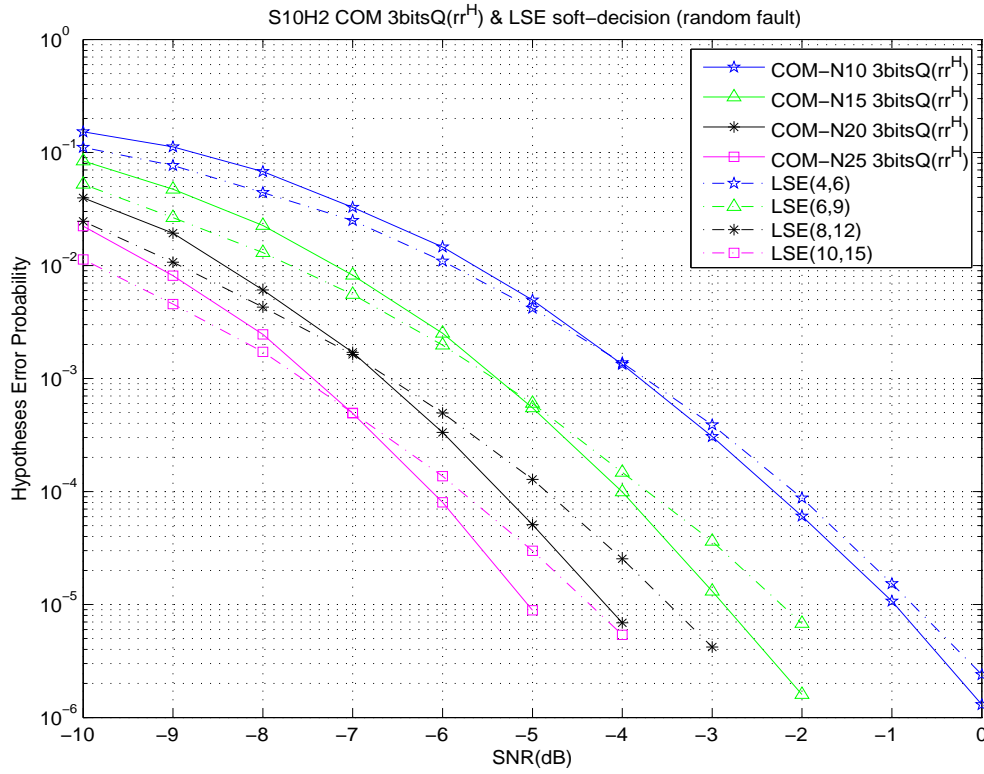


Figure 4.8: Performance of 3-bit product-quantized COM fusion and LSE fusion. “S10H2 ... (random fault)” represents ten sensors, two hypotheses and one random faulty sensor are assumed in this figure. “3bitsQ(rr^H)” means 3-bit quantizer is used in the quantization of product reception rr^H .

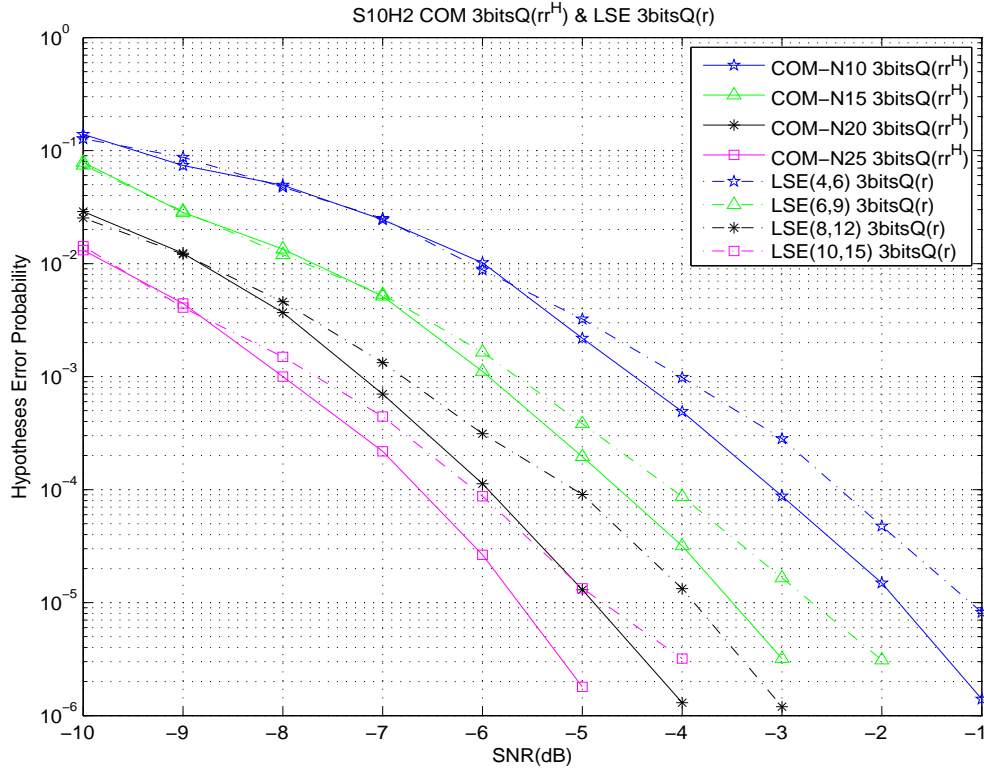


Figure 4.9: Performance of 3-bit reception-product-quantized COM fusion and 3-bit quantized LSE fusion. “S10H2” represents ten sensors and two hypotheses are assumed in this figure. “3bitsQ(rr^H)” means 3-bit quantizer is used in the quantization of product reception rr^H .

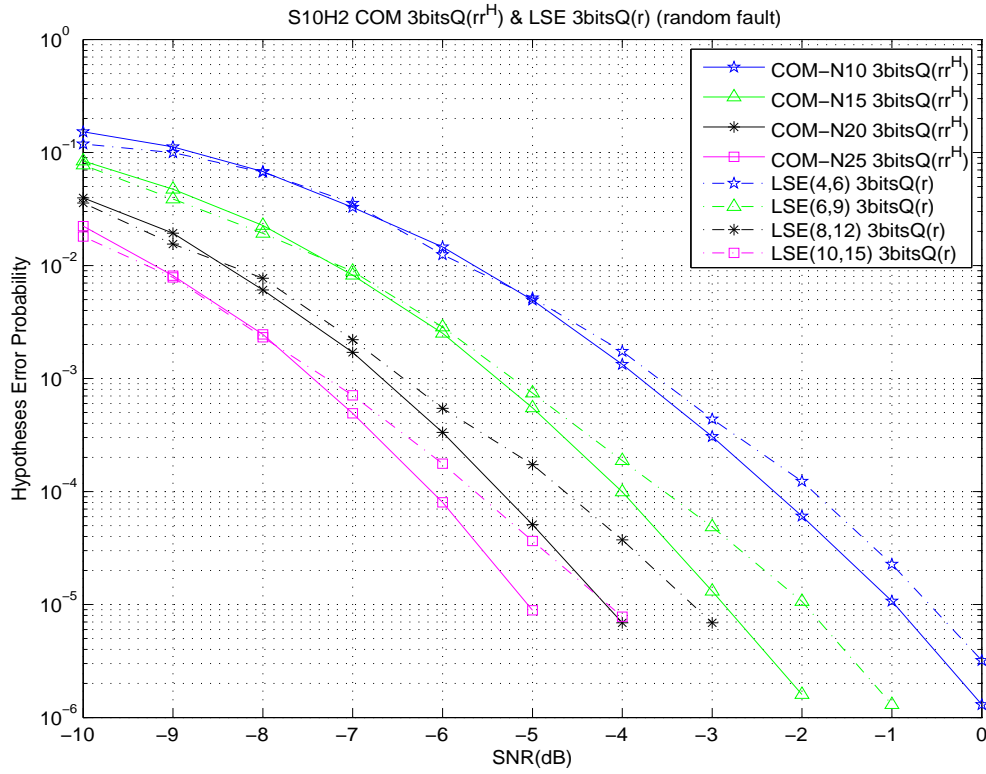


Figure 4.10: Performance of 3-bit reception-product-quantized COM fusion and 3-bit quantized LSE fusion. “S10H2 ... (random fault)” represents ten sensors, two hypotheses and one random faulty sensor are assumed in this figure. “3bitsQ(rr^H)” means 3-bit quantizer is used in the quantization of product reception rr^H .

Chapter 5

Conclusions

In this thesis, the scheme of combined channel estimation and sensor fault protection in wireless sensor networks is examined. Since the training sequence is retained for information-bearing, the simulations indicate that a better performance over the conventional scheme with training-sequence-based channel estimation is resulted. The error floor levels owing to random sensor faults are also less severe in the scheme of combined channel estimation and sensor fault protection. Nevertheless, the sudden performance degradation due to deep fading suggests that quantization at the fusion is more robust than the soft-decision fusion. And quantize rr^H is more robust than quantize r .

Bibliography

- [1] I. F. Akyildiz, W. Su, Y. Sankarasubramaniam, and E. Cayirci, "A survey on sensor networks," *IEEE Communications Magazine*, pp. 102-114, August 2002.
- [2] J. N. Al-Karaki and A. E. Kamal, "Routing techniques in wireless sensor networks: a survey," *IEEE Wireless Communication Magazine*, vol. 11, no. 6, pp. 6-28, 2004.
- [3] P.-N. Chen, T.-Y. Wang, Y. S. Han, P. K. Varshney, and C. Yao, "Performance analysis and code design for minimum hamming distance fusion in wireless sensor networks," *IEEE Trans. Inform. Theory*, vol. 53, no. 5, pp. 1716-1734, May 2007.
- [4] D. Culler, D. Estrin, and M. Srivastava, "Overview of sensor networks," *IEEE Computer*, vol. 37, no. 8, pp. 41-49, Aug. 2004.
- [5] L. Dan, K. D. Wong, H. H. Yu, and A. M. Sayeed, "Detection, classification, and tracking of targets," *IEEE Trans. Signal Processing*, vol. 19, no. 3, pp. 17-29, Mar. 2002.
- [6] R. M. Gray, D. L. Neuhoff, "Quantization," *IEEE Trans. Inform. Theory*, vol. 44, no. 6, pp. 2325-2383, October 1998.
- [7] J. P. Imhof, "Computing the distribution of quadratic forms in normal variables," *Biometrika*, vol. 48, no. 3-4, pp. 419-426, 1961
- [8] S. Kirkpatrick, Jr., C. D. Gelatt, and M. P. Vecchi, "Optimization by simulated annealing," *Science*, vol. 220, no. 4598, pp. 671-680, 1983

- [9] F. Sivrikaya and B. Yener, "Time synchronization in sensor networks: a survey," *IEEE Network*, vol. 18, no. 4, pp. 45-50, Jul.-Aug. 2004.
- [10] M. Skoglund and S. Parkvall, "Code Design for Combined Channel Estimation and Error Protection," *IEEE Trans. Inform. Theory*, vol. 48, no. 5, pp. 1162-1171, May 2002.
- [11] Harry L. Van Trees, *Detection, Estimation, and Modulation Theory*, Volume I, 1993
- [12] T.-Y. Wang, Y. S. Han, B. Chen, P. K. Varshney, "A combined decision fusion and channel coding scheme for distributed fault-tolerant classification in wireless sensor networks," *IEEE Trans. wireless communications*, vol. 5, no. 7, pp. 1695-1705, July 2006.
- [13] C.-L. Wu, P.-N. Chen, Y. S. Han, M.-H. Kuo "Maximum-Likelihood Priority-First Search Decodable Codes for Combined Channel Estimation and Error Protection," *IEEE Trans. Inform. Theory*, to appear.

